

Dear Ran,

We thank you for your insightful comments. I detail below the last modifications done to the manuscript considering your remarks. Hope you will find it relevant.

Hope you are safe despite ongoing covid19 outbreak,
Best,

On behalf of the authors,
Delphine Tardif

Editor: Line 44 – 45: "...From this definition, several broad monsoonal regions can be identified over the globe (Zhang and Wang, 2008; Zhisheng et al., 2015), amongst which the Asian Monsoon system, which is itself declined into smaller monsoonal regions (Wang and LinHo, 2002)."

This sentence is a bit awkward.

Suggested change: ...can be identified over the globe (Zhang and Wang, 2008; Zhisheng et al., 2015). A prominent member is the Asian Monsoon System, which covers several smaller monsoonal regions (Wang and LinHo, 2002).

The authors: Thank you for the suggestion, we changed this sentence accordingly (Lines 50-51)

Editor: Line 55 – 56: ... it is supposed to be enhanced by orographic insulation...

Please replace "supposed" with "thought".

The authors: Done (Line 61)

Editor: Line 74: The use of "doubthouse" is not that common. Please remove the word "often".

The authors: Done (Line 80)

Editor: Line 133 – 134: please keep the acronyms consistent. "IPSL-CM5A-LR" was not used before.

The authors: Indeed, it was replaced by "IPSL-CM5A", previously introduced at Line 147 (Line 149)

Editor: Line 219 – 220: please also check for studies on changing sea water U_{K37} and Mg/Ca values through time, e.g., Tierney & Tingley, (2018, PP) and Tierney et al., (2019 GRL).

The authors: thank you for the suggestion. We propose the following modifications (Lines 237- 242):

« Regarding the proxies, seasonal bias (towards summer or winter, Schouten et al., 2013; Tierney and Tingley, 2018) might affect the temperatures interpreted as representative of the mean annual sea surface temperature. Calibration methods can also be questioned, especially for warmer than present deep-time studies, as it the case for Mg/Ca paleothermometer that doesn't account for the changing Mg/Ca ratio of seawater (Tierney et al., 2019), or for the U_{K37} , for which recent BAYSPLINE recalibration method have proven to lower the mismatch at high temperatures (Tierney and Tingley, 2018). In the case of the TEX₈₆, a subsurface bias has been suggested (Ho and Laepple, 2016) and remains debated (Tierney et al., 2017). »

Editor: Line 231 – 232: there were previous studies on the sensitivity of simulated Eocene

temperature to western U.S. topography. Two examples are Sewall and Sloan (2006, *Geology*) and Feng et al., (2016 *EPSL*).

The authors: thank you, we added the two references (Line 262)

Editor: Line 238: moist adiabatic lapse rate is typically ~5 K/km. 6.5K/km is the global mean lapse rate of present-day. Please clarify.

The authors: 5K/km

Editor: Line 238 – 242: ...Considering a moist adiabatic lapse rate of ~6.5°C/km, this suggests the presence of a temperature bias in this region, regardless of the match with modeled values that may themselves be biased...

This sentence is confusing. The conveyed information is a repetition of the previous sentence. Please consider removing it.

The authors: sentence suppressed as suggested below

Editor: Line 330: "...regimes, the amount of precipitations simulated is biased towards aridity, especially..."

Please replace "biased towards aridity" with "underestimated".

The authors: Done (Line 393)

Editor: Line 333: "...hampers a quantitative comparison to paleovegetation records, which mostly provide estimates of required precipitation amounts."

It is unclear what "required precipitation amounts" meant. Please consider removing the whole "which mostly provide estimates of required precipitation amounts".

The authors: the term "required" may be misleading. We simply explain that paleovegetation studies often provide Mean annual Precipitations values, together with very large uncertainties (that can sometimes double the proposed value). This makes it complicated to compare model precipitation outputs to these Mean Annual Precipitation values retrieved from the data.

We propose to replace "which mostly provide estimates of required precipitations amounts" by "which mostly provide estimates of mean annual precipitations amounts". (Line 396)

Editor: Line 351, Please consider replacing "experiments" with "experiences".

The authors: Done (Line 437)

Editor: Line 445: Please consider replacing "stress out" with "point out".

The authors: Done (Line 537)

Editor: Line 452: Consider replacing "probably intimately" with "closely".

The authors: Done (Line 544)

Editor: Line 458: Replace "rather recent specific" with "more recently developed".

The authors: Done (Line 554)

Editor: Line 462: ...explain the measured patterns (Botsyun et al., 2019; Poulsen et al., 2010). Two additional references are recommended here: Shen et al., (2019, *Clim. Past.*) and Brady et al., (2019, *JAMES*)

The authors: thank you for the suggestion, we have added these references as well as Risi et al. 2010, *JGR* (Line 558)

Editor: Line 462 to 465: The discussion of proxy forward modeling of ice core is out of place. For Deep time, ice core is not an option. Please replace this discussion with something more

deeptime appropriate (e.g., Schmidt 1999, PP; Zhou et al., Zhou et al., 2008 PP; Tindall et al. 2010, EPSL)

The authors: this is correct. However, Zhou et al. 2008 PP and Tindall et al. 2010 EPSL rather describe isotope-enabled models for calculation of seawater past $d^{18}O$ than integration of a proxy transformation of this signal. Therefore, we suggest to replace the paragraph by the following (Lines 559-564):

“Additionally, the application of proxy forward modelling methods (Evans et al., 2013; Schmidt, 1999), by mimicking the mechanisms through which a particular proxy will record a climatic perturbation (e.g. the translation of water $\delta^{18}O$ variations by planktonic foraminifera) taking into account the proxy’s specificity (e.g. ecology of the foraminifera, episodes of secondary calcification and dissolution) and the time uncertainty could contribute greatly to help fill the gap between proxy records and model results.”

Editor: Fig 5: The units for the integrated moisture flux is typically m/s or kg m²/s, an example is Seager and Henderson (2013, J. Clim.). Please check your calculation and write down the equation used here in the figure caption.

The authors: indeed, the unit was wrongly written. The figure displays the northward moisture transport vertically integrated over the whole atmospheric column. It is defined as the mass-weighted vertical integral of the product of northward wind by total water mass per unit mass. The unit was therefore corrected to “kg.m⁻¹.s⁻¹”.

Also, we precised in the call for this Figure in the text: “Figure 5 shows the northward moisture transport vertically integrated over the whole atmosphere column for the Control and EOC4X experiments.” at Line 305

As well as in the Figure legend: “(a, b) Vertically integrated northward JJA moisture transport averaged between 2°S and 2°N (black lines and left axis);” Line 604

Equation:

$$\vec{Q} = -\frac{1}{g} \int_{p_s}^0 q \vec{V} dp$$

where q is the specific humidity and V is the horizontal wind vector, g represents gravitational acceleration and ps stands for surface pressure.

Editor: Fig. 8: Please use uniform legend for both subplots given that they are plotting the same variable.

The authors: Done

Editor: Fig. 10 The purple outline shows in magenta color in my screen. Please consider using a different color.

The authors: the color is indeed magenta, it’s a confusion in translation, “purple” was replaced by “magenta” in the text. Line 649

Paper: <https://doi.org/10.5194/cp-2019-144>

Object: Answer to anonymous referee #1

Dear referee,

Thank you for allowing us to go forward in the publication process. We hereby answer to comments and propose a corrected version of the manuscript. You'll find below the answer to the suggested corrections point by point.

Delphine Tardif, on behalf of the co-authors

[Line 304-305, not only the model bias, but also uncertainties in topography reconstructions, can cause the dry discrepancy in South Asia.](#)

⇒ We propose the following precision at lines 325-327 : "This could be attributed either to a bias towards aridity in these specific regions, that is shared by most models (Valdes et al., 2017) and seems to translate in the Eocene as well, and/or to an inaccurate reconstruction of northern Indian late Eocene topography."

[Line 462, the number 5 is missing in the caption.](#)

⇒ Done

[Line 486, Figure 8 should be replotted. Please check that the purple line does not match with the shaded area in \(a\). It is better to add the simulated precipitation against with these sedimentological records in the Figure 8, since these records could also reflect dry or wet conditions on the orbital time scale, not only the seasonality.](#)

⇒ Figure 8 is replotted. We will join the proxies against MAP in Supplementary information, Figure 7.

Dear referee,

Thank you for allowing us to go forward in the publication process. We hereby answer to comments and propose a corrected version of the manuscript. You'll find below the answer (in black) to the suggested corrections and comments (in blue) point by point.

Delphine Tardif, on behalf of the co-authors

1 The authors conclude there were no modern-like Asian monsoons based on atmospheric circulation (Fig. 4) rather than precipitation seasonality (Fig. 8) in the Eocene simulation. I think it is necessary to have criteria of what atmospheric patterns can be viewed as modern-like monsoons or not. Otherwise, one may argue that Fig. 4c also shows a modern-like monsoon pattern since there is still cross-equator circulation over the Indian ocean though it locates at much lower latitudes.

⇒ The cross equatorial circulation is indeed simulated at very low latitudes in our late Eocene experiment, over India and SE Asian Peninsula. However, we stress in the paper that this cross-equatorial circulation is deviated to the East at a lower latitude in the Eocene than in the modern climate (Fig. 4c-d). This pattern already dismisses the existence of EAM and suggest a weaker SAM. We also did apply the Webster-Yang Index over the region where the cross-equatorial flow is observed and we showed in the original submitted ms. that values obtained for the late Eocene were significantly lower than modern ones (Lines 355-364 and Figure 9).

In order to make our point stronger, we have added the water column integrated moisture flux crossing the equator (Lines 290-300, Figure 5) where the opposite pattern between the control and the Eocene simulation is clearly visible. In particular, one can see that most moisture transport goes from the Indian ocean to the African continent during the Eocene in the 30°E – 60°E sector. To the contrary, the South East Asian monsoon remains well represented in the Eocene (60-90°E).

2 When explaining the Eocene atmospheric circulation (section 3.2), I suggest considering some existing monsoon theories (Boos and Kuang 2010), in which low-level enthalpy or equivalent potential temperature is more physically fundamental to cause circulation and convection anomaly than “blocked by the Tethysian high in Line 267” and “mid-level atmospheric layers very dry and prevents air masses to reach...” in Line 280. Generally, we can say that without the blocking of the TP and Iranian Plateau, cold air is easy to intrude the Indian subcontinent and does not allow building up strong positive low-level enthalpy anomaly, thus not triggering much convection as today.

⇒ We have added a similar diagnostic as the one proposed by Boos and Kuang 2010, i.e. the temperature (in °K) at 300 hPa (see Figure 8 in the revised version). We show that continental Asia is not the main source of heat for the upper troposphere in the Eocene (Fig 8 a), but rather the western Pacific, which contrasts strongly with the modern case (Fig 8b: Control Simulation and SI Fig 6s, ERA5 reanalysis). See Lines 350-354 and Figure 8. This also confirms our first interpretations that the High Pressure – Low Pressure zonation and location in the Eocene induces a cascade of events leading to the absence of deep convection over the Himalaya – Tibetan Plateau system.

3 I feel like the word “onset” (of Asian monsoons) is confusing. I know that it refers to the beginning of the modern-like monsoons over the geological time scales, but it is also usually used to represent the starting time (day or month) of the summer monsoon season and actually authors use this meaning in Line 144. I suggest replacing “onset” with “origin” or other synonyms.

⇒ We thank the reviewer for this suggestion and have replaced the word “onset” by synonyms

4 The authors discuss the model-data comparison problem and point out the importance of correct interpretations of paleo-records. One way to better fill in the gaps between model and proxy records is by using isotope-enabled models (e.g., comparing simulated precipitation isotope ratios to proxies based on precipitation isotopes) and proxy forward modeling (e.g., translating climate variables of simulations directly to pseudoproxies). It would be great if authors can add discussion about this.

⇒ We thank the reviewer; a paragraph has been added stating that (l. 516-524):

“Also, rather recent specific modelling techniques could be very promisingly applied as a complement to complex climatic modelling reconstructions. For example, isotopic-enabled models, by simulating paleoprecipitations $\delta^{18}\text{O}$, allow a direct comparison of the model output to $\delta^{18}\text{O}$ values that can be measured in a wide variety of proxies (shells, carbonates, etc.) and therefore provide robust physical mechanisms to explain the measured patterns (Botsyun et al., 2019; Poulsen et al., 2010). Additionally, the application of proxy forward modelling methods (Dee et al., 2016; Evans et al., 2013), by mimicking the mechanisms through which a particular proxy will record a climatic perturbation (e.g. the translation of a precipitation decrease in an ice core) taking into account the proxy’s specificity (e.g. ice compaction and diffusion) and the time uncertainty could contribute greatly to help fill the gap between proxy records and model results.”

Line 71: These findings “postpone”... Is it “postpone” or “bring forward”?

⇒ They postpone from 22Ma to 40Ma the inception of monsoons

Line 75: «doubthouse» -> “doubthouse”

⇒ Done

Line 98: “A third mechanism”: It is not a mechanism but a conjecture (or other synonyms)

⇒ Done

Line 128: expend -> expand

⇒ Done

Line 136: improved -> improves

⇒ Done

Line 218-221: Cloud feedbacks can also contribute to the model bias: Zhu, J., Poulsen, C. J., & Tierney, J. E. (2019). Simulation of Eocene extreme warmth and high climate sensitivity through cloud feedbacks. *Science Advances*, 5(9), eaax1874. <https://doi.org/10.1126/sciadv.aax1874>

⇒ Indeed. We have added this point and this reference (see Line 222-224)

Line 270: I don’t see easterly winds from the Pacific Ocean

⇒ In Fig 4c, the Asian east coast receives westerlies (>30°N) and weak easterlies (<30°N, northern part of Southeast Asian Peninsula). We have clarified the sentence (see line 302-303).

Line 272: Theses-> These

⇒ Done

Line 275: How to determine the condensation height? The condensation can occur at multiple layers at a single time in the model.

⇒ It is the minimal altitude of condensation, corresponding to an approximation of clouds base level

Line 282: Figure 5->6?

⇒ Done

Line 283: “multiple deep convection”: how do you identify convection here? By upward motion?

⇒ Yes

Line 283: add “center” between humidity and around

⇒ Done

Line 320-325: Do these records all represent precipitation seasonality/seasonal contrast or annual mean precipitation?

⇒ They all suggest highly seasonal precipitations. Some also provide Mean Annual Precipitations estimates, but we choose to focus on seasonality because it appears to be a more robust criteria, as explained at Line 393.

Line 392-393: “When oriented in a NW-SE orientation”: change one of the “orient” words

⇒ Done

All figures: please enlarge the font size of labels of latitude/longitude/color bar. It is especially important for Figure 7.

⇒ Done

Figure 2: How do you calculate sea level pressure anomaly? Is it seasonal mean minus annual mean? Are winds climatological mean or anomalies?

⇒ Yes and yes, we’ve modified the Figure legend to be more specific.

Line 462: Please add “5” before “Pondaung”

⇒ Done

It would be great to add a figure like Figure 5 (a)(b) but in the summer monsoon season in the supplements

⇒ Done, is now in Figure 5c-d

The origin of Asian Monsoons: a modelling perspective

Supprimé: onset

Delphine Tardif¹, Frédéric Fluteau¹, Yannick Donnadieu², Guillaume Le Hir¹, Jean-Baptiste Ladant³,
Pierre Sepulchre⁴, Alexis Licht⁵, Fernando Poblete⁶, Guillaume Dupont-Nivet^{7,8}

¹ Université de Paris, Institut de physique du globe de Paris, CNRS, 75005 Paris, France

² Aix-Marseille Univ, CNRS, IRD, Coll France, INRA, CEREGE, Aix-en-Provence, France.

³ University of Michigan, Ann Arbor, MI, USA

⁴ Laboratoire des Sciences du Climat et de l'Environnement, LSCE/IPSL, CEA-CNRS-UVSQ, Université Paris-Saclay,
91191 Gif-sur-Yvette, France

⁵ University of Washington, Seattle, USA

⁶ Departamento de Geología, Universidad de Chile, Santiago, Chile

⁷ Univ. Rennes, CNRS, Géosciences Rennes, 35000 Rennes, France

⁸ Institute of Geosciences, Universität Potsdam, Germany

Supprimé: ² Centre Européen de Recherche et d'Enseignement des Géosciences de l'Environnement, CEREGE, 13545 Aix-en-Provence, France

Abstract. The Cenozoic inception and development of the Asian monsoons remain unclear and have generated much debate, as several hypotheses regarding circulation patterns at work in Asia during the Eocene have been proposed in the last decades. These include a) the existence of modern-like monsoons since the early Eocene; b) that of a weak South Asian Monsoon (SAM) and little to no East Asian Monsoon (EAM) or c) a prevalence of the Inter Tropical Convergence Zone (ITCZ) migrations, also referred to as Indonesian-Australian Monsoon (I-AM). As SAM and EAM are supposed to have been triggered or enhanced primarily by Asian paleogeographic changes, their possible inception in the very dynamic Eocene paleogeographic context remains an open question, both in the modeling and field-based communities. We investigate here Eocene Asian climate conditions using the IPSL-CM5A2 earth system model and revised paleogeographies. Our Eocene climate simulation yields atmospheric circulation patterns in Asia substantially different from modern. A large high-pressure area is simulated over the Tethys ocean, which generates intense low tropospheric winds blowing southward along the western flank of the proto Himalayan Tibetan plateau (HTP) system. This low-level wind system blocks, to latitudes lower than 10°N, the migration of humid and warm air masses coming from the Indian Ocean. This strongly contrasts with the modern SAM, during which equatorial air masses reach a latitude of 20-25°N over India and southeastern China. Another specific feature of our Eocene simulation is the widespread subsidence taking place over northern India in the mid troposphere (around 5000 m), preventing deep convective updraft that would transport water vapor up to the condensation level. Both processes lead to the onset of a broad arid region located over northern India and over the HTP. More humid regions of high seasonality in precipitations encircle this arid area, due to the prevalence of the Inter Tropical Convergence Zone (ITCZ) migrations (or Indonesian-Australian Monsoon, I-AM) rather than monsoons. Although the existence of this central arid region may partly result from the specifics of our simulation (model dependence, paleogeographic uncertainties) and has yet to be confirmed by proxy records, most of the observational evidence for Eocene monsoons are located in the highly seasonal transition zone between the arid area and the more humid surroundings. We thus suggest that a zonal arid climate prevailed over Asia before the initiation of Monsoons that most likely occurred following Eocene paleogeographic changes. Our results also show that precipitation

Supprimé: onset

Supprimé: onset

seasonality should be used with caution to infer the presence of a monsoonal circulation and that the collection of new data in this arid area is of paramount importance to allow the debate to move forward.

1. Introduction

Monsoons are characterized by highly seasonal precipitations, with a dry season in winter and a wet season in summer, along with a seasonal wind inversion (Wang and Ding, 2008). From this definition, several broad monsoonal regions can be identified over the globe (Zhang and Wang, 2008; Zhisheng et al., 2015). A prominent member is the Asian Monsoon system, which covers several smaller monsoonal regions (Wang and LinHo, 2002). The South Asian Monsoon (SAM) is characterized by dry winters and wet summers with rainfall occurring from May (in southern India and Southeastern Asia) to July (in northwestern India). The East Asian Monsoon (EAM) presents more contrasted seasons with cold and dry winters due to the presence of the Siberian High, and hot and wet summers with rainfall maxima from May (southeastern China) to July (northeastern China). The Indonesian-Australian Monsoon (I-AM), mirrored in the North by the mostly oceanic Western Northern Pacific Monsoon (WNPM), results from the seasonal migration of the Inter Tropical Convergence Zone (ITCZ) and generates rainfall from April to August (over southeastern Asia and western Pacific) and from November to February (over Indonesia and northern Australia).

The ITCZ is an intrinsic characteristic of the Earth's climate and the WNPM and I-AM have therefore probably occurred throughout Earth's history (Spicer et al., 2017). On the other hand, the triggering factors of both SAM and EAM are more complex and remain debated. Although the SAM is also related to the migration of the ITCZ, it is thought to be enhanced by orographic insulation provided by the Himalayas (Boos and Kuang, 2010), by the overheating of the Tibetan Plateau (TP) in summer, and by the generation of a strong Somali jet (Molnar et al., 2010), which might itself be amplified by the East African coast's orography (Bannon, 1979), although this view has been challenged (Wei and Bordoni, 2016). Another characteristic feature of the SAM is a strong shear zone between the 850 and 200 mb zonal winds (Webster and Yang, 1992). In contrast, the EAM is an extra-tropical phenomenon, where winter and summer monsoons are mainly triggered by differential cooling and heating between the huge Asian continental landmass and the western Pacific Ocean, even though it has been suggested that the EAM might also be affected by the Somali Jet strength and TP uplift (Tada et al., 2016).

The inception of the SAM and EAM has been proposed to have occurred during the early Miocene (Guo et al., 2002) or the latest Oligocene (Sun and Wang, 2005) but recent field observations have suggested an earlier inception, as soon as the middle to late Eocene (~40 Ma). These studies rely on different indices such as a) records of high seasonality in precipitations from paleovegetation and sedimentary deposits in China (Quan et al., 2012; Sorrel et al., 2017; Q. Wang et al., 2013) and Myanmar (Licht et al., 2015); b) $\delta^{18}\text{O}$ measurements showing high annual variability in water availability in oyster shells from the Tarim Basin (Bougeois et al., 2018; Ma et al., 2019), in mammals tooth enamel and gastropod shells from Myanmar (Licht et al., 2014). These findings postpone the initiation of the Asian monsoons by about 20 Myr and, given the strong dependence of both SAM and EAM to paleogeography, orography and temperature gradients, raise a challenge of understanding the triggering factors of these complex atmospheric systems in the climatic and paleogeographic context of the middle to late Eocene.

Indeed, the second half of the Eocene, referred to as "doubthouse", is a key period in the transition from the warm ice-free early Eocene greenhouse to colder icehouse initiated in the early Oligocene (Liu et al., 2009). It witnessed profound climatic modifications, such as a global cooling and drying, the possible onset of the Antarctic Circumpolar Current

Supprimé: , amongst which

Supprimé: is itself declined into

Supprimé: supposed

Supprimé: onset

Supprimé: onset

Supprimé: often

Supprimé: «

Supprimé: »

Code de champ modifié

91 (ACC) and a large-scale glaciation in Antarctica (Sijp et al., 2014), hence prefiguring the ~~dawning~~ of modern climatic
92 features. Moreover, important paleogeographic changes took place in the Late Eocene in Asia following the collision
93 between the Eurasian and Indian continents, that might have significantly impacted both regional and global climate;
94 including a) two Paratethys sea retreat with fluctuations phases between 46 and 36 Ma (Meijer et al., 2019); b) the drying
95 and subsequent closure of the India foreland basin (Najman et al., 2008) and c), continued uplift of the Tibetan Plateau
96 (Kapp and DeCelles, 2019).

97 If no consensus has been reached so far regarding the possibility of modern-like SAM and EAM in the Eocene, and on
98 the mechanisms at stake during this period, several conjectures have emerged in the last decades. With the NCAR CCSM3
99 fully coupled model, Huber and Goldner, (2012) suggest that the global monsoon system (including the Asian monsoons)
100 prevailed throughout the Eocene. Using a Late Eocene configuration and the Fast Ocean Atmosphere Model (FOAM)
101 along with LMDZ atmosphere model, Licht et al., (2014) postulate the existence of the Asian monsoons in the late Eocene
102 and show that orbital forcing might even trigger monsoons stronger than the modern ones. Other studies have also inferred
103 the existence of the Asian monsoons in the late Eocene on the basis of sensitivity experiments deriving mainly from
104 modern geographic configurations (Roe et al., 2016; Zoura et al., 2019).

105 Other studies, although more focused on the EAM, are more cautious regarding the prevalence of the monsoons in the
106 Eocene. Zhang et al., (2012) using FOAM suggest that early Eocene Asia was dominated by steppe/desert climates, with
107 a stable SAM but only an intermittent EAM depending on the orbital forcing. Li et al., (2018) and Zhang et al., (2018)
108 perform late Eocene climate simulations with the low-resolution NorESM-L Earth System Model (ESM) and the NCAR
109 CAM4 atmospheric model and further show that the wind and precipitation patterns simulated in eastern China are not
110 comparable to the modern EAM.

111 A third ~~theory~~ has also recently been suggested based on both modeling work (Farnsworth et al., 2019) and leaf
112 physiognomic signatures from vegetation deposits from southeastern China, which is a region nowadays experiencing a
113 mixed influence of EAM, I-AM and SAM (Herman et al., 2017; Spicer et al., 2016). They show that the fossil floras from
114 the Maoming and Changchang basins display more similarities with modern floras submitted to the influence of I-AM
115 than to that of any other monsoon, hence suggesting that ITCZ migration could have been the main driver of precipitation
116 seasonality in the late Eocene.

117 The discrepancies between these different conjectures are hardly straightforward, given the variety of modeling
118 framework, model resolution and boundary conditions involved in the aforementioned studies, let alone considering the
119 possible biases of any model. From an observational perspective, available paleoclimatic markers in Asia are also divided
120 between proxies suggesting the presence of Eocene monsoons and others that do not. However, the uncertainties
121 associated with the climatic controls of the diverse proxies used to infer the existence of Eocene Asian monsoons often
122 hamper the unequivocal assignment of the proxy signals to the monsoons.

123 In this study, we first test the robustness of our ESM by analyzing monsoonal circulations for modern conditions. The
124 use of an ESM here is particularly indicated given the importance of atmosphere-SST interactions in monsoon circulation.
125 We then simulate the late-middle Eocene (42 to 38 Ma) climate using a 40 Ma paleogeographic reconstruction. First, we
126 perform a global model-data comparison with both continental and marine temperatures, allowing us to demonstrate the
127 ability of our model to simulate the late Eocene climate at the first order. Second, we analyze atmospheric circulation
128 patterns over Asia and highlight potential (di-)similarities with modern circulation. We finally focus on the atmospheric
129 dynamics and on the hydrological cycle features occurring over the Asian continent during the late Eocene, and discuss
130 the possible reasons behind the discrepancies observed between the different existing hypotheses.

Supprimé: onset

Supprimé: mechanism

Code de champ modifié

133 2. Model and methods

134 2.1. Model description and validation

135 IPSL-CM5A2 (Sepulchre et al., 2019) is composed of the atmospheric LMDZ5 model (Hourdin et al., 2013), the land
136 surface ORCHIDEE model (Krinner et al., 2005) and the NEMO model including oceanic, biogeochemical and sea-ice
137 components (Madec, 2016). The atmospheric grid has a resolution of 3.75° (longitude) by 1.89° (latitude) and 39 vertical
138 layers from the surface up to 40 km high and the tripolar oceanic grid has a resolution varying between 0.5° to 2° and 30
139 vertical layers. The continuity of the processes at the interface between ocean and atmosphere is ensured by the OASIS
140 coupler (Valcke et al., 2006). The land surface ORCHIDEE model is coupled to the atmosphere with a 30 mn time-step
141 and includes a river runoff module to route the water to the ocean (d'Orgeval et al., 2008). Vegetation is simulated through
142 eleven Plant Functional Types (hereafter PFT): eight forest PFTs, one bare soil PFT and two grasses PFTs, one coding
143 for C₃ grasses and the other one for C₄ grasses (Poulter et al., 2011). As the C₄ plants are known to expand during the late
144 Miocene (Cerling et al., 1993), this last PFT was deactivated.

145 IPSL-CM5A2 is an updated version of IPSL-CM5A (Dufresne et al., 2013), which was already used in paleoclimate
146 studies for the Quaternary (Kageyama et al., 2013) and the Pliocene (Contoux et al., 2012; Tan et al., 2017). It relies on
147 more recent versions of each component, and has been re-tuned to reduce the IPSL-CM5A global cold bias. Apart from
148 retuning - that is based on a new auto conversion threshold for water in cloud - and various improvements in energy
149 conservation, the LMDZ component of IPSL-CM5A2 has the same physics and parameterizations than IPSL-CM5A.
150 Jet position and AMOC have been improved, together with the sea-ice cover. IPSL-CM5A2 also benefits from higher
151 parallelization (namely MPI-OpenMP in the atmosphere), which improves the model scalability and allows the model to
152 reach ~100 years per day simulated on the JOLIOT-CURIE French supercomputer (Sarr et al., 2019; Sepulchre et al.,
153 2019). We nonetheless first provide a validation of the model on modern climatic conditions for the Asian monsoon
154 regions.

155 We evaluate IPSL-CM5A2 ability to reproduce the climate patterns over Asia by comparing the last 20 years of a 1855-
156 2005 historical run (Sepulchre et al., 2019) to the Global Precipitation Climatology Project (GPCP) for rainfall, and to
157 the European Centre for Medium-Range Weather Forecasts (ECMWF) reanalysis (ERA-40) for the winds (Frauenfeld,
158 2005). Regarding precipitation, IPSL-CM5A2 shows typical biases shared with CMIP5-generation models, i.e. a ca. 2-
159 month delay in the monsoon onset over India (see Supplementary materials, Figure 1), an underestimated extension of
160 the monsoon over eastern China, Korea, and Japan, and an overestimation of rainfall rates over the subtropical
161 western/central Pacific Ocean and Indian ocean (Sperber et al., 2013). However, these biases are reduced in IPSL-CM5A2
162 compared to the previous IPSL ESM version (Dufresne et al., 2013), as a response to a tuning-induced better SST pattern
163 over the Arabian Sea that enhances rainfall over India during the summer monsoon (Levine et al., 2013).

164 Simulated mean annual precipitation (MAP) rates fits the main patterns of GPCP (Figure 1-a,b), although IPSL-CM5A2
165 tends to expand aridity over Arabia and Central Asia. Rainfall amounts over Nepal and Bangladesh are underestimated,
166 whereas they are reinforced over the foothills of the Himalayas, likely as a response to the lack of spatial resolution that
167 prevents representing orographic rainfall associated with the steep changes in topography of these regions. The expression
168 of seasonality, calculated through the ratio of the precipitations during the 3 consecutive wettest month against the 3
169 consecutive driest month (hereafter 3W/3D) is well represented over Asia (Figure 1-c,d). We have chosen the 3W/3D
170 ratio among many available criteria to characterize the climate seasonality because it has also been used as an indicator

Supprimé: c

Supprimé: -LR

Supprimé: d

of monsoonal climates (with a minimum threshold value close to 5) in previous investigations of paleo-monsoons (Herman et al., 2017; Shukla et al., 2014; Sorrel et al., 2017). The modern monsoonal regions in our model are adequately characterized by a high 3W/3D ratio, although this signature is stronger in southern Asia than in eastern China. The seasonality in precipitation is thus consistently reproduced for the modern. Regarding atmospheric large-scale dynamics, winter monsoon winds are well simulated, with anticyclonic winds around the Siberian high (Figure 2-a,b). The summer circulation patterns (Figure 2-c,d) are also well reproduced, although the low pressure belt over Arabia and southern Asia is simulated with lower intensity and lesser extension than in the reanalysis. Likewise, the simulated EAM intrusion in eastern China appears to be less pervasive than in the reanalysis, in which winds coming from the South China Sea penetrate further inland. The simulated Somali Jet and SAM winds display weaker intensity, but mirrors the patterns observed in the reanalysis. Given that IPSL-CM5A2 reproduces well the seasonal atmospheric dynamics patterns and the seasonality, we will thus mostly focus on these criteria in the discussion that follows.

2.2. Late Eocene fully coupled simulation set up

The Eocene simulation (EOC4X) uses a 40 Ma paleogeography and paleobathymetry reconstruction (see Supplementary materials, Figure 2-a). Global plate reconstructions follow methods and plate references described in Baatsen et al., (2016) with significant modifications in tectonically active area within the 45-35 Ma based on a review of geologic data and literature (<https://map.paleoenvironment.eu/>). Specifically in the India-Asia collision zone, paleopositions are based on paleomagnetic references (Lippert et al., 2014) and collision is underway with greater India completely emerged (Najman et al., 2010). Based on a review of geological constraints (see Botsyun et al., (2019); Kapp and DeCelles, (2019) and references therein), the Tibetan Plateau altitude is set to 3500 m in Central Tibet forming a high elevated low-relief plateau. Moderate-low-elevation paleosurface for Northern Tibet and low-elevated regions further north into the Qaidam and Tarim Basins (surrounded by very subdued topography below 1000 m for the mountain belts of the Pamir, Kunlun Shan, Tian Shan, Altyn Shan and Qilian Shan / Nan Shan) decrease finally into the plain and epicontinental sea of Central Asia. The Paratethys is set to its extent estimated during the maximum ingression reached just before 41 Ma (Bosboom et al., 2017) and the Turgai strait, which connected the Paratethys sea and the Arctic Ocean, is set closed by mid Eocene (Akhmet'sev and Beniamovski, 2006; Kaya et al., 2019), but the water exchanges with the Tethys ocean are maintained to the south.

The CO₂ atmospheric concentration is set to 1120 ppm (4 PAL or 4X interchangeably), which corresponds to the high end of middle to late Eocene (42 - 34 Ma) pCO₂ estimates from data and carbon cycle models (Anagnostou et al., 2016; Beerling and Royer, 2011; Lefebvre et al., 2013). Ice sheets are removed as the presence of even small permanent ice sheets was highly unlikely under these CO₂ concentrations (DeConto and Pollard, 2003; Gasson et al., 2014). As other greenhouse gases (CH₄, NO₂, O₃) concentrations are poorly constrained for this period, they are left to their preindustrial values, as proposed in model intercomparison projects on pre-Quaternary periods (Lunt et al., 2017). The solar constant is reduced to 1360.19 W/m² (Gough, 1981) and the orbital parameters are set to their present values.

Although several vegetation reconstructions are proposed in the literature for the Eocene, they were usually designed for higher CO₂ concentrations (e.g. 8 PAL, in Herold et al., 2014) and/or different paleogeographies, such as the early Eocene (Sewall et al., 2000). Here, our Eocene fully coupled simulation uses an idealized vegetation map derived from the main

211 modern climatic zones on the globe (see Supplementary materials, Figure 2-b). The limits of this approach will be
212 discussed in the Discussion section.

213 3. Results

214 We first compare the simulated oceanic and terrestrial temperatures to two compilations of SST and mean annual
215 terrestrial temperatures (MAT), ranging respectively from 42 to 38 Ma (late-middle Eocene) and to 38 to 34 Ma (late
216 Eocene, a complete description of the compilation is given in the supplementary materials, Table 1 to 4). The main
217 climatic patterns over Asia obtained for EOC4X simulation are then presented and compared to the modern, and we
218 discuss potential implications on our understanding of the Cenozoic monsoon history.

219 3.1. Comparison of the simulated Eocene climate with a proxy compilation

220 The EOC4X ocean is initialized from warm idealized conditions similar to that proposed by (Lunt et al., 2017) and has
221 been run for 3000 years. At the end of the integration the ocean has reached quasi-equilibrium, including in the deep
222 oceanic layers, showing a drift inferior to 0.05 °C per century (see Supplementary Materials Figure 3). Our reference
223 simulation yields SST in better agreement with the 42-38 Ma late-middle Eocene group than with the late Eocene group
224 (Figure 4 in Supplementary materials). This suggests that our 4 PAL results are more representative of the late-middle
225 Eocene conditions, which seems consistent given the fact that 4 PAL corresponds usually to the higher CO₂ estimates for
226 the second half of the Eocene. Consequently, we develop here the comparison with the late-middle Eocene proxy group
227 (Figure 3), and attach the comparison between model and late Eocene proxy group (Supplementary Materials, Figure 5).
228 The comparison with SST estimates yields overall good results, although some discrepancies remain: at high latitudes,
229 DSDP 277 near New Zealand and ODP 913 in the North Atlantic show temperatures warmer by ~13°C compared to the
230 model, while in the Gulf of Mexico, the proxy is 11°C cooler than the model and in the equatorial Atlantic (site ODP 925)
231 proxies are 8°C cooler than the model. Despite a steeper latitudinal thermal gradient than that reconstructed from proxy
232 records, the model is able to match reasonably well the coldest and warmest proxy values (respectively 8° for the ACEX
233 drilling, in the Arctic and 36°C for JavaKW01 on the equator) with a +/- 3.5°C accuracy. This conundrum, where models
234 struggle to reproduce the flatter thermal gradient suggested by proxy records by simulating too warm (resp. cold)
235 temperatures at the equator (resp. poles), is a recurrent problem in modeling studies. Underlying causes remain unclear
236 and could be attributed to proxy uncertainties, missing processes in the models, (Huber and Caballero, 2011) or biases in
237 the way models handle small-scale processes, such as cloud feedbacks (Zhu et al., 2019). Regarding the proxies, seasonal
238 bias (towards summer or winter, Schouten et al., 2013; Tierney and Tingley, 2018), might affect the temperatures
239 interpreted as representative of the mean annual sea surface temperature. Calibration methods can also be questioned,
240 especially for warmer than present deep-time studies, as it the case for Mg/Ca paleothermometer that doesn't account for
241 the changing Mg/Ca ratio of seawater (Tierney et al., 2019), or for the U^K₃₇, for which recent BAYSPLINE recalibration
242 method have proven to lower the mismatch at high temperatures (Tierney and Tingley, 2018). In the case of the TEX₈₆,
243 a subsurface bias has been suggested (Ho and Laepple, 2016) and remains debated (Tierney et al., 2017). In Asia, δ¹⁸O
244 measurements in oyster shells from the eastern edge of the Paratethys sea spanning the second half of the Eocene give
245 estimates for the mean annual temperature as well as the seasonal amplitude, yielding SST estimates ranging from 22°C

Supprimé: , such as biases or

Supprimé: and proxy uncertainties

Supprimé: , remain unclear

Supprimé: For instance

Code de champ modifié

Supprimé: Schouten et al., 2013)

Supprimé: proxy-based

Mis en forme : Non Surlignage

Mis en forme : Non Surlignage

Mis en forme : Non Surlignage

Mis en forme : Non Surlignage

Mis en forme : Non Exposant/ Indice, Non Surlignage

Mis en forme : Non Surlignage

Mis en forme : Non Surlignage

Supprimé: or,

Supprimé: i

254 in winter to 38°C in summer (Bougeois et al., 2018). The simulated SSTs are consistent with these values, with a coldest
 255 simulated SST of 15°C in January and a warmest simulated SST of 35°C in August.

256 The fit between modeled and terrestrial proxies MAT (Figure 3-c,d) is less successful. The model reasonably fits
 257 temperatures in Australia, South America, Antarctica, Greenland and Europe with a mismatch between values staying
 258 below +/-5°C for all locations, except the Gran Barranca (Chile) and Stare Seldo I (Europe) points. On the other hand,
 259 larger differences exist over North America and Asia, although the mismatch might likely have different origins. All of
 260 North American proxy sites are located close to the West coast and to the Rocky Mountains, the Cenozoic history of
 261 which is also complex. Incorrect prescribed topography in the model as well as local effects of atmospheric circulation
 262 might therefore have a large impact in terms of reconstructed temperatures (Feng and Poulsen, 2016; Sewall and Sloan,
 263 2006). We note that the model successfully represents the proxy temperature range in this region (between 3 and 23°C
 264 for the proxies and between 4 and 27°C for the model), which suggests that the model-data mismatch is more likely
 265 related to paleoelevation errors or local climatic effects rather than to a systematic bias in either the model or proxies. On
 266 the contrary, the remarkable homogeneity amongst the estimated MAT from Asian proxy records (ranging only from 14
 267 to 19°C) is somewhat puzzling, considering the fact that these 28 sites are spread between 18 and 52°N in latitude and
 268 are located in various geographical settings, ranging from coastal regions to mountainous areas. A possible cause could
 269 be the application of modern temperature-vegetation relationships to paleobotanical records, which might not prove fully
 270 adequate to reconstruct the warmer climates of the Eocene (Grimm and Potts, 2016; Peppe et al., 2011).

271 If quantitative comparisons between model and paleovegetation data need to be treated with caution for climates warmer
 272 than modern, fossilized plants, together with lithological proxies, do however provide useful qualitative information. In
 273 Asia, Eocene proxy reconstructions converge towards a generally zonal climatic pattern, with a dry arid belt spreading
 274 from the Tarim basin to the east coast of China (Sun and Wang, 2005), and fringed by more humid climates over India
 275 and South East Asia on its southern flank (Licht et al., 2014; Ma et al., 2012; Sun and Wang, 2005) and over Siberia to
 276 the North (Akhmetiev and Zaporozhets, 2014). In the next sections, we will focus on the atmospheric circulation simulated
 277 for our Eocene simulation and analyze the shape and occurrence of the different Asian monsoons.

278 3.2. Asian Eocene atmospheric circulation

279 EOC4X seasonal atmospheric circulation patterns are presented for winter (December-January-February) (Figure 4-a)
 280 and summer (June-July-August) (Figure 4-c) and compared to their modern counterparts (Figure 4-b,d). The winter
 281 circulation is characterized by a strong high-pressure belt at latitudes lower than today, located over the proto Himalayan
 282 Tibetan Plateau between 20 and 45°N. Strong westerlies are simulated at mid-latitudes around 40-50°N and easterlies at
 283 latitudes lower than 20°N (up to 15 m/s against 5 m/s in the Control simulation). These features contrast with the modern
 284 winter system characterized by zonal winds with a lower intensity and a larger meridional component. Finally, no
 285 analogue to the modern Siberian High is simulated at 40 Ma (Figure 4-b). Today, the Siberian High is controlled by winter
 286 surface temperatures dropping below the freezing point in northeastern Siberia (around 50°N). In our Eocene simulation,
 287 the combined effect of a warmer climate and a reduced continentality (due to the presence of the Paratethys and Siberian
 288 seas) prevent its development.

289 During summer months, the nearby presence of the Tethys ocean and Paratethys sea results in a large high-pressure cell
 290 centered over 30°E and extending from 10° to 50°N (Figure 4-c). The Tethysian high is associated with intense 850 mb
 291 northerlies around 60°E which are partly deviated into northwesterlies when sweeping over northern Greater India (Figure

Supprimé: Considering a moist adiabatic lapse rate of ~5°C/km, this suggests the presence of a temperature bias in this region, regardless of the match with modeled values that may themselves be biased.

Supprimé: zonal winds blow eastward

Supprimé: westward

Supprimé: formation

Supprimé: is

Supprimé: southward

Supprimé: winds

4-c). To the south, 850 mb winds originated from the Indian Ocean enter the Indian subcontinent at low latitudes ($<10^{\circ}\text{N}$) and turn southeasterlies over the Bengal Bay to feed precipitations over the foothills of Himalaya before shifting to southwesterlies (Figure 4-c). In the modern configuration, the 850 mb winds of the SAM originate from the Indian Ocean and extend northward up to 20°N over India before taking a northeast direction and generate heavy precipitations from India to Myanmar and up to the southern flank of the Himalayas to the North (Figure 4-d, Figure 5-d). These precipitations over southern Asia (up to 15 mm/day, Figure 5-d) are fed by the Somali Jet, a strong low-level cross-equatorial moisture flow originating from the Indian Ocean which turns anticyclonically in the northern hemisphere along the eastern edge of the eastern African relief (Figure 4-d).

Figure 5 shows the northward moisture transport vertically integrated over the whole atmosphere column for the Control and EOC4X experiments. In the Control Experiment, the largest meridional moisture transport crossing the Equator is simulated along the Eastern African coastline (Figure 5-b) and corresponds to the strongest meridional wind component. It confirms that the Somali Jet is a key feature of the modern Southern Asian Monsoon (Figure 5 b,d). Conversely in the EOC4X experiment, the Somali Jet ($0-10^{\circ}\text{N}/45-50^{\circ}\text{E}$) barely exists. Instead, moisture flows from the Tethys and Indian Oceans towards western Africa, where heavy summer precipitations are simulated (over 30 mm/day, Figure 5 c). This alternate moisture pathway toward western Africa rather than southern Asia is probably the result of several paleogeography features (African continent positioned farther south, absence of topography in eastern Africa, presence of a Tethys seaway preventing the south Asian low pressure to extend westward) and will be discussed further in Section 4.2.

In the western Indian ocean, the cross-equatorial moisture flow is strongly reduced in EOC4X compared to the Control simulation, whereas it is increased over the eastern Indian ocean. However, this diverted equatorial moisture flux remains below 10°N and the Asian eastern Pacific coast receives instead a mixture of westerly winds coming from northern India (above 30°N) and weak easterly winds bringing moisture from the Pacific Ocean at lower latitudes (Figure 5c), contrasting strongly with the modern EAM (Figure 5d).

These atmospheric changes, both in summer and winter, generate a large arid area extending throughout western China, the proto-Tibetan Plateau and northern India, while southern India and Myanmar experience intense rainfall due to their position closer to the equator in the Eocene (Figure 6a,b). Apart from changes in near surface winds, two intertwined processes conspire to explain the aridity: (1) a rise in the water vapor condensation height (corresponding roughly to the cloud base), and (2) a weakly convective atmospheric column. The first process arises from the extreme surface air temperature in EOC4X (up to 45°C), which results in a simulated water condensation altitude that exceeds 3500 m over Northern India and Tibet. This altitude corresponds to a pressure level of ~ 680 mb (in the middle troposphere), while the water condensation altitude remains below 2500 m in the control experiment, which corresponds to a pressure level of ~ 800 mb (in the lower troposphere, Figure 6c,d). The second process, the lack of deep convection, makes mid-level atmospheric layers very dry and prevents air masses to reach the water condensation altitude, as shown by two longitude-altitude cross sections of the relative humidity at 20°N and at 40°N (Figure 7).

At 20°N today, modern India and Southeast Asia show multiple deep convection centers and a relative humidity around 60% in most of the troposphere (Figure 7d). In contrast, the Eocene displays a more stratified atmosphere, with two weak convective cells above the Indian and Southeastern Asian land masses, which are blocked around 600 mb by subsiding air masses. Locations of deep convective heating can also be highlighted by observing the upper troposphere temperature maxima in the tropics (Boos and Kuang, 2010; Privé and Plumb, 2007; Roe et al., 2016), as presented in Figure 8. In the Control experiment, upper temperature maxima are located over northern India deep convection regions (Figure 8-b).

Supprimé : which prevent northward penetration of warm and humid air masses coming

Mis en forme : Retrait : Première ligne : 0 cm

Supprimé : In the modern configuration, these air masses, which constitute the SAM system, move northward up to 20°N before taking a northeast direction and generate heavy precipitations from India to Myanmar and up to the southern flank of the Himalayas to the north (Figure 4-d). In EOC4X, these winds are weaker and their northward advection is rapidly blocked by the Tethysian high that persists all year round (Figure 4-c). Similarly, weaker winds coming from the Bay of Bengal in EOC4X are diverted toward the northwest to feed precipitations over the foothills of Himalaya before shifting to a more northeast direction.

Supprimé : The eastern

Supprimé : of China, under the influence of the EAM at the present time,

Supprimé : 4

Supprimé : which

Supprimé : s

Supprimé : 4

Supprimé : s

Supprimé : 5

Supprimé : vertical level

Supprimé : 5

Supprimé : 5

Supprimé : Moreover,

Supprimé : 6

Mis en forme : Police : 10 pt, Couleur de police : Noir

369 which is in good agreement with reanalysis (see SI, Figure 6). Deep convection tends to occur where latent and sensible
 370 heats per unit mass maximize which is close to the subcloud surface (Emanuel et al., 1994), where temperature and
 371 relative humidity are elevated. In the control experiment, deep convection over India appears to be mostly controlled by
 372 latent heat because evaporation of precipitated water ensures moisture availability. Yet, in EOC4X, the latent heat over
 373 India is largely weaker due to a lack of moisture despite warmer temperatures. Consequently no upper-level temperature
 374 peak is simulated over northern India but rather over the Western Pacific (Figure 8-a), where both temperature and relative
 375 humidity are the highest.
 376 At 40°N, the presence of the Paratethys sea and the Tarim basin as far as 80°E is translated into a shallow surface of high
 377 relative humidity (~70%, see Figure 7-a), which is confined in the lowest troposphere levels by strong subsiding winds.
 378 The deep convection is here again muted by large-scale mid-level atmospheric dynamics. These diagnostics converge to
 379 demonstrate that our simulated Eocene atmosphere in Asia has little in common with the modern. The application of the
 380 Webster and Yang Index (WYI) (Webster and Yang, 1992) further confirms these atmospheric contrasts. The WYI is a
 381 standard diagnostic criterion for the SAM that quantifies the shear effect between the lower and higher troposphere, which
 382 is a typical characteristic of this monsoon. Modern WYI summer values over the northern Indian Ocean exceeds 20
 383 whereas our EOC4X simulation yields summer values below 6 (Figure 9), thereby emphasizing the strong differences
 384 between Eocene and modern summer circulation patterns in this region.

385 4. Discussion

386 4.1. Can proxies identify monsoons?

387 The comparison of our model results showing a broad arid zone over Asia, with late Eocene proxy records is reasonably
 388 good despite the fact that many of these records have been used to infer the existence of monsoons. This is first shown
 389 by a simple qualitative comparison with vegetation reconstructions from the Middle Eocene (Figure 6-a), derived from a
 390 compilation of paleobotanical studies (detailed in supplementary materials). The spatial distribution of forests and
 391 shrubland/grassland inferred from these studies is mostly coherent at first order with simulated MAP, however, a
 392 discrepancy remains between the northern Indian and Bengal forests and the dry conditions simulated (< 1mm/day). This
 393 could be attributed either to a bias towards aridity in these specific regions, that is shared by most models (Valdes et al.,
 394 2017) and seems to translate in the Eocene as well, and/or to an inaccurate reconstruction of northern Indian late Eocene
 395 topography. We have indeed shown that, although our model reasonably simulates the modern monsoons in a control
 396 simulation in terms of wind regimes, the amount of precipitations simulated is underestimated, especially in India and in
 397 the Bengal region (Figure 1-a,b). This, together with the large error bars associated with most of the quantitative
 398 reconstructions on precipitations proposed by paleobotanical studies, hampers a quantitative comparison to
 399 paleovegetation records, which mostly provide estimates of mean annual precipitation amounts. We thus rather focus on
 400 Eocene proxy records of seasonality (as previously done in Huber and Goldner, 2012), for example as of our model's
 401 ability to produce seasonality metrics in good agreement with modern observations (Figure 1-c,d).
 402 Figure 8 shows the 3W/3D obtained with EOC4X and compared to the Late-Middle Eocene compilation of coal and
 403 evaporites deposits from Boucot et al., (2013). In the literature, evaporites are traditionally interpreted as markers of
 404 seasonal to arid environment, while coals indicate more stably wet climates, and thus have been extensively relied on to
 405 infer past climates (Huber and Goldner, 2012; Sun and Wang, 2005; Ziegler et al., 2003). However, this approach has

Supprimé: the moist static energy is maximum in the subcloud atmospheric boundary layer (Emmanuel et al., 1994; Roe et al., 2016) that is where

Supprimé: .

Supprimé: Yet, i

Supprimé: as a

Supprimé: ce

Supprimé: of the shallow convection cells

Supprimé: shown before

Supprimé: ,

Supprimé: observed

Supprimé: The latent heat over India is largely weaker than in the Control experiment due to the lack of moisture and the sensible heat cannot compensate despite the warmer temperature in the

Supprimé: 1

Mis en forme : Police :10 pt

Supprimé: 6

Supprimé: 7

Supprimé: 5

Supprimé: can

Supprimé: common

Supprimé: biased towards aridity

Supprimé: required

429 been criticized as oversimplistic (Wang et al., 2013; Williams, 2007). Therefore, in addition to this compilation, we
 430 highlighted localities positioned in strategic regions and resulting from robust multi-proxy analysis, that were recently
 431 used to suggest monsoon-like highly seasonal climatic conditions during the late-middle Eocene (Figure 10a): 1) the
 432 Tarim region (Bougeois et al., 2018); 2) the Xining Basin, located at the interface between the zones of influence of the
 433 modern westerlies and of the EAM (Meijer et al., 2019); 3) the Maoming/Changchang basins in southeastern China
 434 (Herman et al., 2017; Spicer et al., 2016), located in the transition zone between EAM and I-AM; 4) the Jiuziyan
 435 Formation (Sorrel et al., 2017) and finally 5) the Pondaung formation in Myanmar (Licht et al., 2014), presently located
 436 in the area of influence of the SAM. Although we lack Indian sites suggesting the presence of the SAM in the late Eocene,
 437 we acknowledge that such sites do exist for the early Eocene (i.e. the Guhra mine in Rajasthan, Shukla et al., (2014).
 438 When compared to our model results, most of the evaporite deposits and highlighted localities are found in regions of
 439 strong seasonality ($3W/3D > 5$, purple outline in Figure 10a), except for the Myanmar site located in a more ever-wet
 440 context and the Tarim region, which experiences a mostly ever-dry climatic context. As many of these highlighted
 441 localities stand on the edge of our simulated arid zone, we suggest that the extension of this region might be modulated
 442 by orbital forcing, as both models and data seem to suggest (Abels et al., 2011; Licht et al., 2014; Sloan and Morrill, 1998;
 443 Zhang et al., 2012), which should be the topic of further investigations. Inversely, most coal bearing deposits stand in
 444 regions of very low seasonality and relatively high MAP (southern India, southern Myanmar, northeastern China),
 445 although some discrepancies remain in northern India and Bengal regions, which could be linked to the aforementioned
 446 dry bias of the model and/or to regional bias induced by specific coal depositional environment. The comparison of coal
 447 and evaporites deposits to late Eocene MAP, although less reliable for the reasons mentioned above, follow a comparable
 448 pattern, as most of coals settle in regions of relatively high MAP (> 1000 mm/year) while the evaporites, on the other
 449 hand, are present in drier locations (SI, Figure 7).
 450 These results, together with the previously shown wind patterns highlight that Eocene seasonality and wind regimes might
 451 have been substantially different from the modern conditions. We argue that high seasonality criteria ($3W/3D$ or similar)
 452 may equally result from either SAM, EAM, or ITCZ seasonality (WNPM or I-AM), and therefore hardly discriminate
 453 between these different mechanisms. This ambiguity is also apparent in the proxy records. For example, markers of highly
 454 seasonal precipitations found in Myanmar were successively interpreted as indicators of a modern-like SAM (Licht et al.,
 455 2014), then to a migrating ITCZ-driven monsoonal rainfall due to revised paleolatitude of the Burma terrain (Westerweel
 456 et al., 2019). Additional seasonality data in targeted areas as well as the application of new techniques on fossil leaves
 457 (Spicer et al., 2016) that are promising in their ability to distinguish between the different seasonal signals (ITCZ, SAM,
 458 EAM) might in this regard bring meaningful insights on new and existing sites and together with modeling results help
 459 resolve the question of the monsoons initiation timing.

460 4.2. What drove the inception of Asian Monsoons?

461 The atmosphere dynamics over Asia in our Eocene simulation presents significant differences relative to the modern. It
 462 indicates the existence of a latitudinal extensive arid zone over northern India and central Asia bordered by areas of highly
 463 seasonal precipitation, however our results do not produce monsoonal circulations in the modern sense. The absence of a
 464 true paleo-monsoon contrasts with the findings reported in some previous Eocene modeling studies but a large arid zone
 465 is consistent with other model studies of Eocene or other time periods as detailed below. This interestingly suggests that
 466 the boundary conditions necessary for the inception of monsoon-like circulations may have occurred within this broad

Supprimé: 108

Supprimé: 8

Supprimé: experiments

Supprimé: onset

Supprimé: onset

Supprimé: onset

greenhouse timeframe and, more importantly, that the monsoon-triggering conditions may be determined by comparing these various model studies with our results and proxy data. Indeed, each study has its own modeling setup and differences in the results might come from either the choice of model, the model resolution and/or the boundary conditions that were used. If all the CMIP5 generation models, except for CCSM4, experience the same dry bias in Asia when compared to modern observations (Valdes et al., 2017), and if a better resolution appears to have limited impact on the outcoming results (Huber and Goldner, 2012; Li et al., 2018), the paleogeography is a key point to consider. Indeed, recent studies suggest that paleogeography is the key driver shaping eastern Asian climate (Farnsworth et al., 2019) and (Lunt et al., 2016) further showed that paleogeographic changes observed during the Eocene could be responsible for mean annual temperature changes that might be as high as $\pm 6^{\circ}\text{C}$.

Several main diverging paleogeographic characteristics stand out between all the available modelling studies regarding the Eocene. First, the position of the Indian continent, which either is fully disconnected from Asia and in an equatorial position (Huber and Goldner, 2012; Zhang et al., 2012) or has already collided with Asia (this study; Li et al., 2018; Licht et al., 2014; Zhang et al., 2018). Second, the orientation and the latitude of HTP significantly differ from a study to another (Huber and Goldner, 2012; Licht et al., 2014; Zhang et al., 2018). Third, the Turgai strait that is either represented as open (Li et al., 2018; Licht et al., 2014; Zhang et al., 2012) or close (this study, Huber and Goldner, 2012; Zhang et al., 2018). Fourth, the elevation of oriental Siberia, that displays variable elevation ranging from $<1000\text{m}$ (this study, Huber and Goldner, 2012; Zhang et al., 2012) to more mountainous (1000 to 2000 m) configurations (Li et al., 2018; Licht et al., 2014; Zhang et al., 2018). Given that some of these key features of the late Eocene paleogeography are still highly debated (Kapp and DeCelles, 2019, for a review), we propose below a short review of previous studies and the possible impact of varying boundary conditions on resulting Asian climate.

There are competitive models for the evolution of the Indian Foreland seaway, with some predicting the presence of a deep sea between Continental India and Asia (Jagoutz et al., 2015; van Hinsbergen et al., 2012) or an epicontinental sea (DeCelles et al., 1998) in the early and middle Eocene. However, geological evidence indicates that the Indian Foreland seaway have dried out by 40 million years (Najman et al., 2008) and terrestrial connection is suggested even earlier, around 53.7 Ma, according to paleontological evidence based on mammalian fossils (Clementz et al., 2011). In that aspect, the existence of a seaway between India and Asia (Huber and Goldner, 2012; Zhang et al., 2012), is clearly representative of the early Eocene. Regardless of the exact timing for the complete emergence of Greater India, the presence of a seaway in these warm low latitudes certainly represents an important water vapor source to the surrounding regions (Tibetan Plateau, northern India, Bengal), and could therefore reduce the aridity of this area.

Interestingly, the Tethys/Paratethys region from Huber and Goldner, (2012) presents more similarities with the early Miocene, as northern Africa and Arabia are fully emerged while the remnants of the Paratethys sea in Europe are reduced to small inner seas. We hypothesize that the increased continentality in Europe and northern Africa in their experiment may contribute to prevent the formation of a Tethysian anticyclone (as simulated in the present study), hence generating atmospheric circulation more similar to the modern. On the other hand, also with the use of an early Eocene Indo-Asian configuration but a broader Tethys ocean and Paratethys sea, Zhang et al., (2012) obtain results that are more similar to ours in terms of sea level pressure and seasonal winds. This supports the importance of the Paratethys extension in shaping Asian climate, which was already suggested by previous studies (Fluteau et al., 1999; Ramstein et al., 1997; Zhang et al., 2007).

Recent findings suggest that the latitudinal position of the TP exert a control over Eocene Asian climate, especially summer wind patterns (Zhang et al., 2018) and therefore add another level of uncertainty given that the location and

Supprimé: x

514 elevation of the TP in the Eocene is still debated (Botsyun et al., 2019; Wang et al., 2014). When oriented in a NW-SE
 515 ~~direction~~ and located between 10 and 20°N, the TP blocks summer equatorial winds transporting moisture northward and
 516 enhances orographic precipitations over the southern flank of the TP, while westerly winds coming from the Paratethys
 517 cross central Asia without encountering major orographic barriers (Licht et al., 2014; Zhang et al., 2018). On the contrary,
 518 configurations with a modern TP position (between 30 and 40°N) deviate the westerlies coming from the Paratethys into
 519 a counter-clockwise flow around the southern flank of the TP (this study; Zhang et al., 2018).
 520 The Turgai strait configuration and oriental Siberian paleotopography might also have a significant impact on the
 521 simulated Asian climate. An open Turgai Strait (Li et al., 2018; Licht et al., 2014; Zhang et al., 2012) maintains a
 522 connection between the warm Paratethys sea and the colder Northern sea and might result in an increased land-sea thermal
 523 gradient in the western Asian mid latitudes by cooling the Paratethys. Providing that the seaway is deep enough to allow
 524 for such heat exchanges, it could amplify the land-sea breeze phenomenon in summer between the Paratethys and the
 525 Asian continent and play a part in Central Asian water budget. A more mountainous configuration of inner Siberia (Li et
 526 al., 2018; Licht et al., 2014; Zhang et al., 2018) might generate colder winter temperatures and create the conditions
 527 required for the inception of a proto Siberian High in winter. Although the closure of the Turgai strait is estimated to
 528 occur around mid-Eocene (Akhmetiev and Zaporozhets, 2014), Siberian paleoelevation remains highly speculative and,
 529 to our knowledge, neither have been the topics of in-depth modelling studies.
 530 In summary, current knowledge about late Eocene Asian paleogeography is not yet sufficient to discriminate between the
 531 various model solutions obtained with different boundary conditions. Moreover, some models come to the same
 532 conclusions using different paleogeographic reconstructions. This review, however, indicates and identifies potential
 533 paleogeographic boundary conditions have driven the shift from arid zonal Asia to Asian monsoonal conditions. We also
 534 argue that a modeling intercomparison project focusing on late Eocene Asian climate, using similar boundary conditions
 535 and applying similar diagnostic criteria, would definitely be a valuable asset to the community to provide a consistent
 536 picture of the ~~initiation~~ and evolution of Asian monsoons from a modeling perspective.

Supprimé: orientation

Code de champ modifié

Code de champ modifié

Code de champ modifié

Code de champ modifié

Code de champ modifié

Supprimé: onset

537 5. Conclusion

538 The earth system model IPSL-CM5A2 is able to catch modern Asian main climatic features and to produce Eocene
 539 climatic reconstructions which seem realistic when compared to proxy SST estimates and are comparable to recent studies
 540 that proposed a global climate reconstruction for this time period using earth system models (Baatsen et al., 2018;
 541 Hutchinson et al., 2018; Inglis et al., 2015). Our results ~~point~~ out notable differences in terms of wind patterns and
 542 precipitation amounts in Asia when compared to modern circulation, suggesting that no SAM neither EAM were
 543 occurring at that time, although highly seasonal climate is modelled in these regions. Our climate simulation rather
 544 proposes the existence of a wide arid zone in northern India and central Asia, due to the presence of strong subsiding
 545 winds in the mid troposphere, preventing the moist air coming from the equator to condensate and precipitate over the
 546 continent. These simulations suggest that these conditions prevailed before the set-up of the modern SAM and EAM,
 547 more likely appearing after the late Eocene, by contrast to what is found in other simulations (e.g. Huber and Goldner,
 548 2012). If the existence of this arid climate is ~~closely~~ linked to the late Eocene paleogeography, the scarcity of paleo data
 549 in this simulated arid region remains a limitation.
 550 We suggest that investigating the precise period when Asia transitioned from arid zonal climate to modern-like monsoonal
 551 climate would require collecting data in this specific arid area. Ultimately, we believe that additional simulations

Code de champ modifié

Supprimé: stress

Supprimé: probably intimately

556 performed using different models forced by identical boundary conditions as well as new Paleogene records from Asia
557 (especially in southeastern Asia and India) are needed to draw more precise conclusions on the appearance of Asian
558 monsoons and their potential existence in that period. Also, more recently developed modelling techniques could be very
559 promisingly applied as a complement to complex climatic modelling reconstructions. For example, isotopic-enabled
560 models, by simulating paleoprecipitations $\delta^{18}\text{O}$, allow a direct comparison of the model output to $\delta^{18}\text{O}$ values that can be
561 measured in a wide variety of proxies (shells, carbonates, etc.) and therefore provide robust physical mechanisms to
562 explain the measured patterns (Botsyun et al., 2019; Brady et al., 2019; Poulsen et al., 2010; Risi et al., 2010).
563 Additionally, the application of proxy forward modelling methods (Evans et al., 2013; Schmidt, 1999), by mimicking the
564 mechanisms through which a particular proxy will record a climatic perturbation (e.g. the translation of water $\delta^{18}\text{O}$
565 variations by planktonic foraminifera) taking into account the proxy's specificity (e.g. ecology of the foraminifera,
566 episodes of secondary calcification and dissolution) and the time uncertainty could contribute greatly to help fill the gap
567 between proxy records and model results.
568

Code de champ modifié

Supprimé: (Dee et al., 2016; Evans et al., 2013)

Mis en forme : Exposant

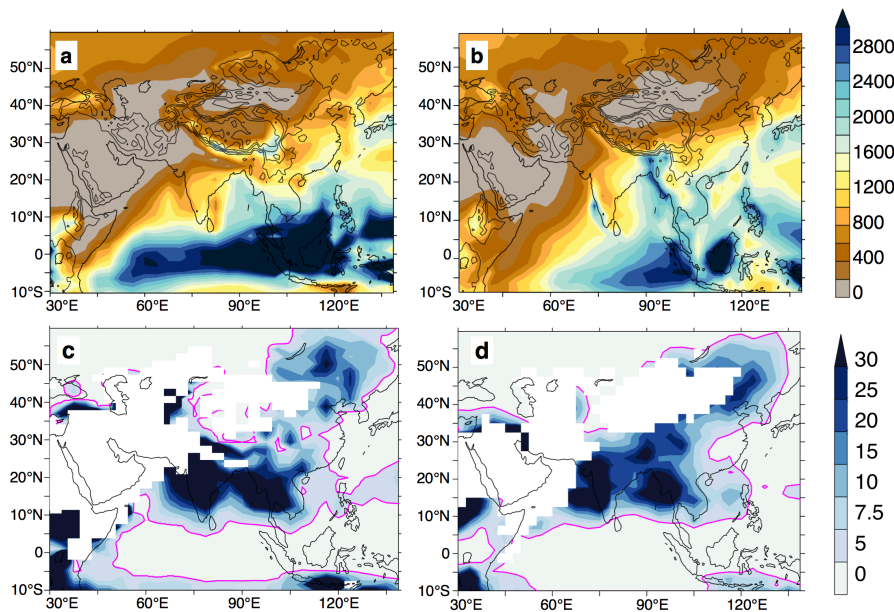
570

571 6. Appendices: Figures

572 Figure 1: Comparison of mean annual precipitations in mm/year (a,b) and 3wet/3dry ratio (c,d) simulated in the
573 modern control simulation (a,c) and the GPCP observations (b,d).

574

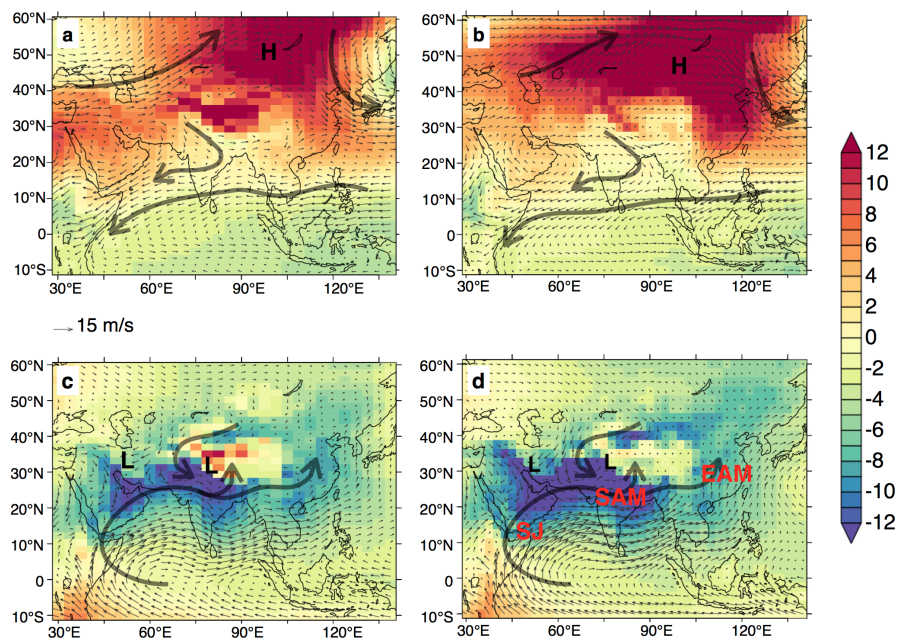
575



576

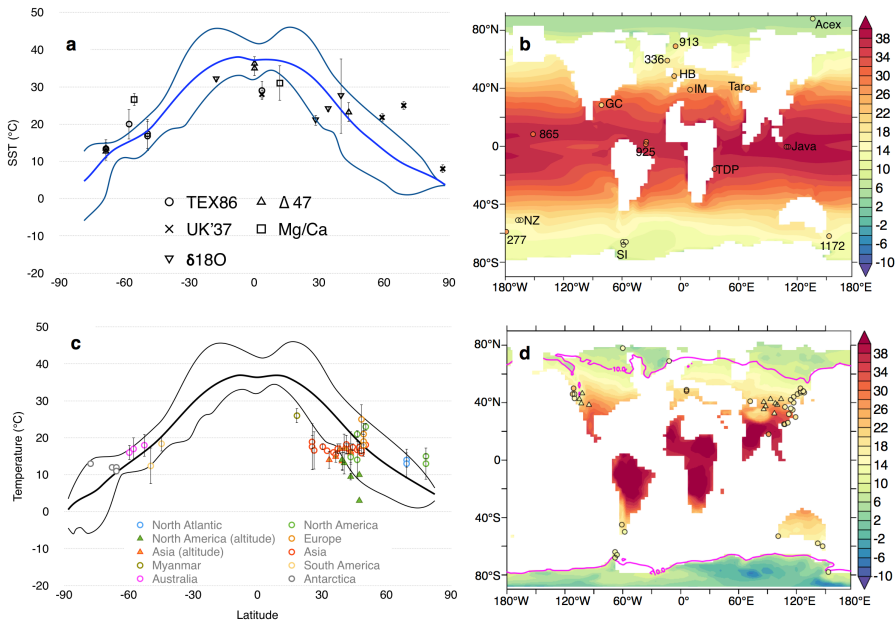
577

578 Figure 2: Comparison of January to March (a,b), June to August (c,d) mean wind patterns obtained in the modern
 579 control simulation (a,c) with ERA40 reanalysis (b,d). Shading represents Sea Level Pressure anomaly (in mb),
 580 calculated as the difference between seasonal SLP minus the mean annual SLP. Overprinted vectors show 850 mb
 581 wind speed expressed in m/s. Main zones of high (low) pressure are highlighted with H (L) black letters. Main
 582 features of the summer monsoon are highlighted in red: Somali Jet (SJ), South Asian Monsoon (SAM) and East
 583 Asian Monsoon (EAM).
 584



588 **Figure 3: Late-middle Eocene global model-data comparison for SST (a,b) and MAT (c,d). In (a, c), thick line**
 589 **represents the mean temperature from EOC4X, thin lines the min and max latitudinal temperatures from EOC4X.**
 590 **For terrestrial proxies (d), high altitude locations (>1000 m) are represented by triangles, the others by circles and**
 591 **pink thick line represent the 10°C isotherm.**
 592

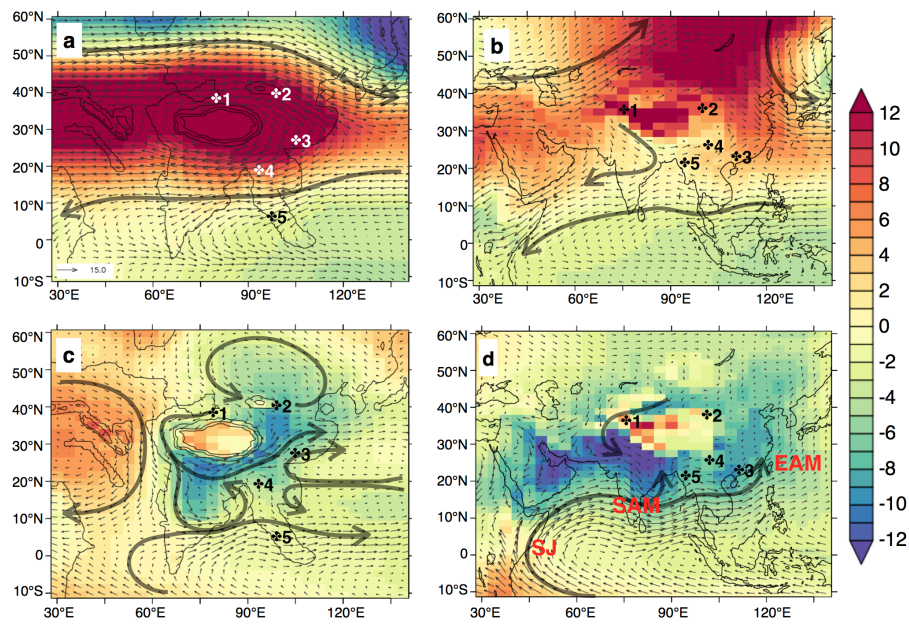
593



594

595

596 Figure 4: Sea level pressure anomaly (shading, in mb) and 850 mb wind patterns (vectors, m/s) obtained in EOC4X
 597 (a,c) and compared to control simulation results (b,c). (a,b) Winter circulation pattern; (c,d) summer circulation
 598 patterns. Main wind patterns are represented by a thick black arrow, and low pressure zones (high pressure) are
 599 marked by letter L (H). Numbers corresponds to regions highlighted in the main text: 1 Tarim sea region (Bougeois
 600 et al., 2018), 2 Xining Basin (Meijer et al., 2019, Licht et al., 2014), 3, Maoming Basin (Herman et al., 2017, Spicer
 601 et al., 2016, 2017), 4 Jiuchuan basin (Sorrel et al. 2017) and 5 Pondaung formation in Myanmar (Licht et al., 2014).
 602



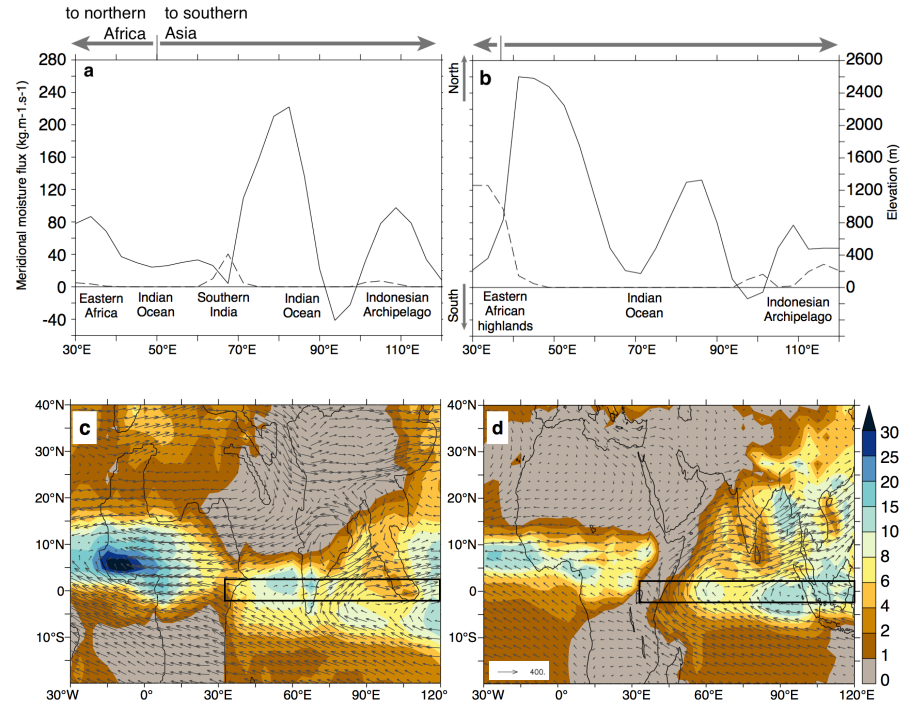
603
 604
 605

606
607
608
609
610
611
612
613
614
615

Figure 5: Comparison of EOC4X (a, c) and Control (b, d) water column integrated moisture fluxes. (a, b) Vertically integrated northward JJA moisture transport averaged between 2°S and 2°N (black lines and left axis) and expressed as:

$$\vec{Q} = -\frac{1}{g} \int_{p_s}^0 q \vec{V} dp$$

where q is the specific humidity and V is the horizontal wind vector, g the gravitational acceleration and ps the surface pressure; dotted lines represent the elevation of land masses within the same latitudinal band (right axis); arrows and legends indicate the direction of the zonal component of moisture fluxes. (c, d) JJA moisture fluxes (vectors) and cumulated precipitations for the same period (mm/day). Black boxes highlight the area used to compute meridional moisture fluxes in (a, b).

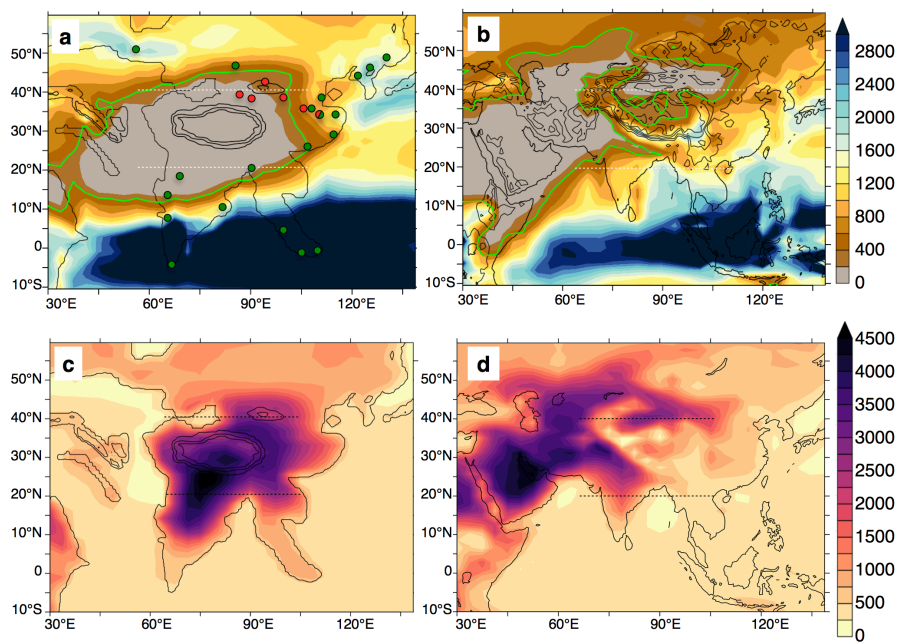


616
617
618

Mis en forme : Police :10 pt, Gras
Mis en forme : Police :10 pt, Gras
Mis en forme : Justifié
Mis en forme : Police :10 pt, Gras
Mis en forme : Police :10 pt, Gras
Supprimé: Figure 5: Comparison of EOC4X (a, c) and Control (b, d) Meridional moisture flux (a, b) (left axis, full black line) averaged between 2°S and 2°N ; dotted line represents the continents position and elevation (right axis) , arrows and legends indicate meridional and zonal direction of the moisture flux. (c, d) mean JJA wind moisture flux (UQ,VQ vectors) and mean monthly precipitations for the same period (mm/day). Black boxes highlight the area used to compute meridional moisture flux in (a, b).
Mis en forme : Couleur de police : Texte 1, Anglais (E.U.)

629 Figure 6: (a,b) Mean annual precipitations (mm/year) for EOC4X simulation (a) and the Control simulation (b).
 630 The green outline delimits the arid region receiving less than 1mm/day. (c,d) Water condensation altitude (in m)
 631 in July for EOC4X simulation (c) and Control simulation (d). Horizontal dotted lines show the latitude used for
 632 the meridional profiles in Figure 5. In (a), circles indicate location of paleovegetation studies and describe forested
 633 environment (green) and shrub/grass environment (red), according to qualitative descriptions described in the
 634 Supplementary Materials (Table 5).

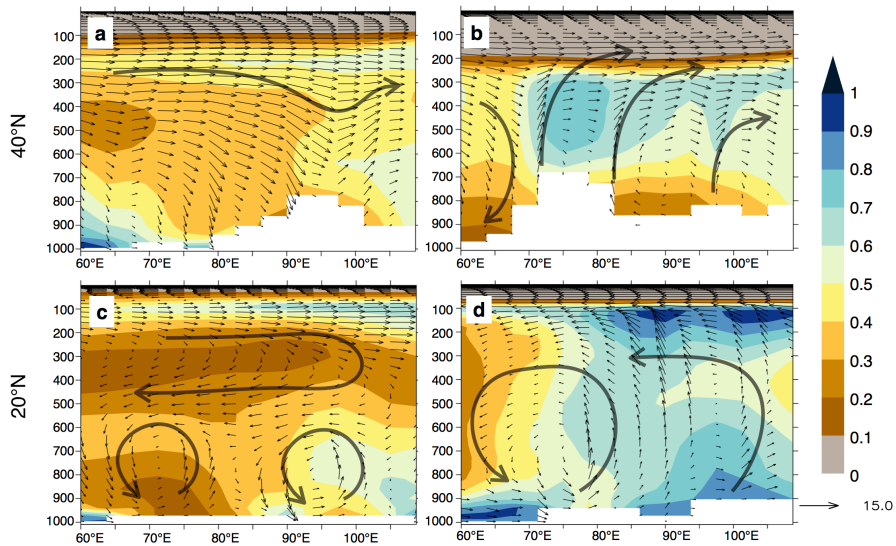
635



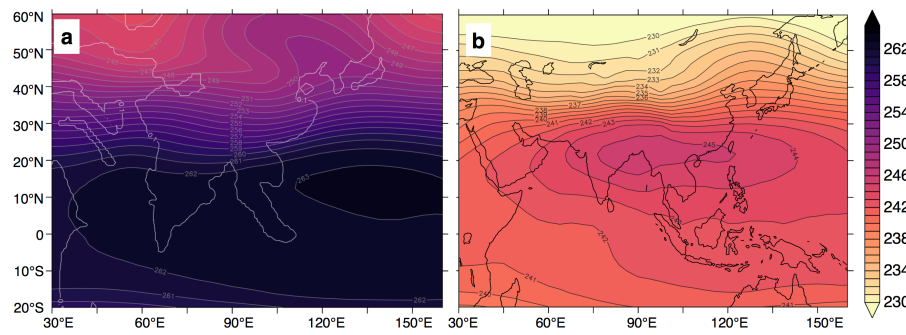
636

637

638 Figure 7: Longitude-Altitude profiles of the relative humidity (shaded) and vertical winds (vectors) for EOC4X
 639 (a,c) and control simulation (b,d), at 40° N and (a,b) and 20° N (c,d). Values are taken from the month of July.
 640

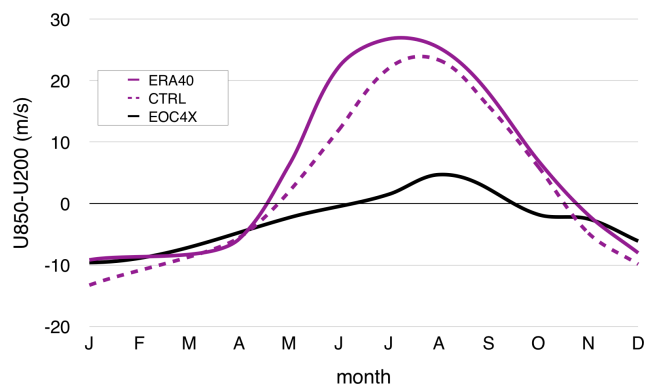


641
 642
 643
 644 **Figure 8: JJA Air Temperature (in Kelvin) at 300 mb for EOC4X (a) and Control (b) with contours overlaid each**
 645 **degree.**
 646

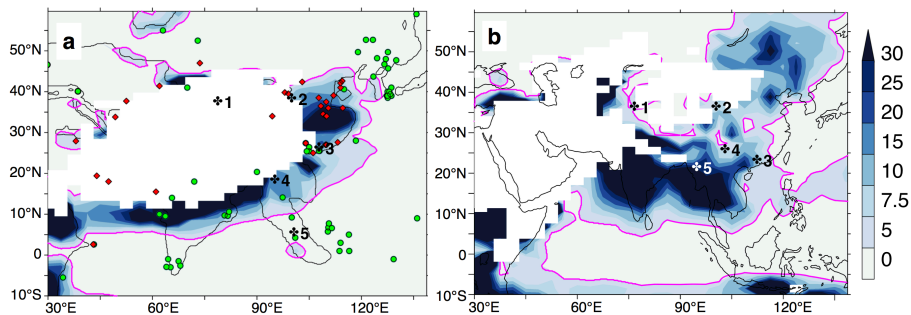


647
 648
 649

650 Figure 9: Application of the Webster and Yang Index (on the region 40 E:110 E, 0:20 N) and comparison of the
 651 results obtained for EOC4X (black), control simulation (dotted) and reanalysis (purple).
 652



653
 654
 655 Figure 10: 3W/3D ratio for EOC4X (a) and Control simulation (b). Regions receiving less than 1mm/day are kept
 656 blank. Overlaid magenta outline corresponds to the value 3W3D=5 considered as minimum value in modern
 657 monsoonal regions. We also highlight evaporite (red diamonds) and coal deposits (green circles) from Boucot et
 658 al. 2013, as well as the five highlighted regions described in the text.
 659



660
 661

662

663 7. Code availability

664 LMDZ, XIOS, NEMO and ORCHIDEE are released under the terms of the CeCILL license. OASIS-MCT is released
665 under the terms of the Lesser GNU General Public License (LGPL). IPSL-CM5A2 code is publicly available through
666 svn, with the following command lines: `svn co`
667 http://forge.ipsl.jussieu.fr/igcmg/svn/modipsl/branches/publications/IPSLCM5A2.1_11192019 modipsl
668 `cd modipsl/util;./model IPSLCM5A2.1`

669 The mod.def file provides information regarding the different revisions used,namely :
670 – NEMOGCMbranchnemo_v3_6_STABLErevision6665 – XIOS2branches/xios-2.5revision1763
671 – IOIPSL/srcsvntags/v2_2_2
672 – LMDZ5branches/IPSLCM5A2.1rev3591
673 – branches/publications/ORCHIDEE_IPSLCM5A2.1.r5307rev6336 – OASIS3-MCT2.0_branch(rev4775IPSLserver)

674 The login/password combination requested at first use to download the ORCHIDEE component is
675 anonymous/anonymous. We recommend to refer to the project website:
676 http://forge.ipsl.jussieu.fr/igcmg_doc/wiki/Doc/Config/IPSLCM5A2 for a proper installation and compilation of the
677 environment.

678 8. Authors contribution

679 DTB, YD and JBL conducted the Eocene experiments. DTB, FF, YD and GLH analyzed the results and realized the
680 discussion.
681 PS, JBL and YD developed the AOGCM version used in this work. FP and GDN reconstructed the Eocene
682 paleogeography.
683 The discussion was further emphasized by the contributions of AL (model-data discussion). PS conducted the Control
684 Simulation and emphasized the model description and the comparison of the Control simulation results with GPCP
685 observations and ERA40 reanalysis. All co-authors contributed to the writing the manuscript.

686 9. Competing interests

687 The authors declare that they have no conflict of interest.

688 10. Acknowledgements

689 ~~The authors thank the two anonymous reviewers and the editor who helped improve the quality of this paper.~~ This work
690 was granted access to the HPC resources of TGCC under the allocation 2018-A0050107601 made by GENCI. This work

Supprimé: ¶

692 was funded by the INSU-CNRS SYSTER. G. D.-N. acknowledges support from ERC MAGIC grant 649081. [This is](#)
693 [IPGP contribution 4115.](#)

694 11. Bibliography

- 695 Abels, H.A., Dupont-Nivet, G., Xiao, G., Bosboom, R., Krijgsman, W., 2011. Step-wise change of
696 Asian interior climate preceding the Eocene–Oligocene Transition (EOT). *Palaeogeography,*
697 *Palaeoclimatology, Palaeoecology* 299, 399–412. <https://doi.org/10.1016/j.palaeo.2010.11.028>
- 698 Akhmetiev, M.A., Zaporozhets, N.I., 2014. Paleogene events in Central Eurasia: their role in the flora
699 and vegetation cover evolution, migration of phytochore boundaries, and climate changes.
700 *Stratigraphy and Geological Correlation* 22, 312–335. <https://doi.org/10.1134/S0869593814030022>
- 701 Akhmet'sev, M.A., Beniamovski, V.N., 2006. The Paleocene and Eocene in the Russian part of West
702 Eurasia. *Stratigraphy and Geological Correlation* 14, 49–72.
703 <https://doi.org/10.1134/S0869593806010047>
- 704 Anagnostou, E., John, E.H., Edgar, K.M., Foster, G.L., Ridgwell, A., Inglis, G.N., Pancost, R.D.,
705 Lunt, D.J., Pearson, P.N., 2016. Changing atmospheric CO₂ concentration was the primary driver of
706 early Cenozoic climate. *Nature* 533, 380–384. <https://doi.org/10.1038/nature17423>
- 707 Baatsen, M., van Hinsbergen, D.J.J., von der Heydt, A.S., Dijkstra, H.A., Sluijs, A., Abels, H.A., Bijl,
708 P.K., 2016. Reconstructing geographical boundary conditions for palaeoclimate modelling during the
709 Cenozoic. *Climate of the Past* 12, 1635–1644. <https://doi.org/10.5194/cp-12-1635-2016>
- 710 Baatsen, M., von der Heydt, A.S., Huber, M., Kliphuis, M.A., Bijl, P.K., Sluijs, A., Dijkstra, H.A.,
711 2018. Equilibrium state and sensitivity of the simulated middle-to-late Eocene climate. *Climate of*
712 *the Past Discussions* 1–49. <https://doi.org/10.5194/cp-2018-43>
- 713 Bannon, P.R., 1979. On the Dynamics of the East African Jet. I: Simulation of Mean Conditions for
714 July. *Journal of the Atmospheric Sciences* 36, 2139–2152. [https://doi.org/10.1175/1520-](https://doi.org/10.1175/1520-0469(1979)036<2139:OTDOTE>2.0.CO;2)
715 [0469\(1979\)036<2139:OTDOTE>2.0.CO;2](https://doi.org/10.1175/1520-0469(1979)036<2139:OTDOTE>2.0.CO;2)
- 716 Beerling, D.J., Royer, D.L., 2011. Convergent cenozoic CO₂ history. *Nature Geoscience* 4, 418–420.
- 717 Boos, W.R., Kuang, Z., 2010. Dominant control of the South Asian monsoon by orographic insulation
718 versus plateau heating. *Nature* 463, 218–222. <https://doi.org/10.1038/nature08707>
- 719 Bosboom, R., Mandic, O., Dupont-Nivet, G., Proust, J.-N., Ormukov, C., Aminov, J., 2017. Late
720 Eocene palaeogeography of the proto-Paratethys Sea in Central Asia (NW China, southern
721 Kyrgyzstan and SW Tajikistan). *Geological Society, London, Special Publications* 427, 565–588.
722 <https://doi.org/10.1144/SP427.11>
- 723 Botsyun, S., Sepulchre, P., Donnadieu, Y., Risi, C., Licht, A., Caves Rugenstein, J.K., 2019. Revised

724 paleoaltimetry data show low Tibetan Plateau elevation during the Eocene. *Science* 363, eaaq1436.
725 <https://doi.org/10.1126/science.aaq1436>

726 Boucot, A.J., Xu, C., Scotese, C.R., Morley, R.J., 2013. *Phanerozoic Paleoclimate: An Atlas of*
727 *Lithologic Indicators of Climate*. SEPM (Society for Sedimentary Geology), Tulsa, Oklahoma,
728 U.S.A. <https://doi.org/10.2110/sepmcsp.11>

729 Bougeois, L., Dupont-Nivet, G., de Rafélis, M., Tindall, J.C., Proust, J.-N., Reichart, G.-J., de
730 Nooijer, L.J., Guo, Z., Ormukov, C., 2018. Asian monsoons and aridification response to Paleogene
731 sea retreat and Neogene westerly shielding indicated by seasonality in Paratethys oysters. *Earth and*
732 *Planetary Science Letters* 485, 99–110. <https://doi.org/10.1016/j.epsl.2017.12.036>

733 Cerling, T.E., Wang, Y., Quade, J., 1993. Expansion of C4 ecosystems as an indicator of global
734 ecological change in the late Miocene. *Nature* 361, 344–345.

735 Clementz, M., Bajpai, S., Ravikant, V., Thewissen, J.G.M., Saravanan, N., Singh, I.B., Prasad, V.,
736 2011. Early Eocene warming events and the timing of terrestrial faunal exchange between India and
737 Asia. *Geology* 39, 15–18. <https://doi.org/10.1130/G31585.1>

738 Contoux, C., Ramstein, G., Jost, A., 2012. Modelling the mid-Pliocene Warm Period climate with the
739 IPSL coupled model and its atmospheric component LMDZ5A. *Geoscientific Model Development*
740 5, 903–917. <https://doi.org/10.5194/gmd-5-903-2012>

741 d’Orgeval, T., Polcher, J., de Rosnay, P., 2008. Sensitivity of the West African hydrological cycle in
742 ORCHIDEE to infiltration processes. *Hydrology and Earth System Sciences* 12, 1387–1401.
743 <https://doi.org/10.5194/hess-12-1387-2008>

744 DeCelles, P.G., Gehrels, G.E., Quade, J., Ojha, T.P., 1998. Eocene-early Miocene foreland basin
745 development and the history of Himalayan thrusting, western and central Nepal. *Tectonics* 17, 741–
746 765. <https://doi.org/10.1029/98TC02598>

747 DeConto, R.M., Pollard, D., 2003. A coupled climate–ice sheet modeling approach to the Early
748 Cenozoic history of the Antarctic ice sheet. *Palaeogeography, Palaeoclimatology, Palaeoecology* 198,
749 39–52. [https://doi.org/10.1016/S0031-0182\(03\)00393-6](https://doi.org/10.1016/S0031-0182(03)00393-6)

750 Dufresne, J.-L., Foujols, M.-A., Denvil, S., Caubel, A., Marti, O., Aumont, O., Balkanski, Y., Bekki,
751 S., Bellenger, H., Benshila, R., Bony, S., Bopp, L., Braconnot, P., Brockmann, P., Cadule, P., Cheruy,
752 F., Codron, F., Cozic, A., Cugnet, D., de Noblet, N., Duvel, J.-P., Ethé, C., Fairhead, L., Fichet, T.,
753 Flavoni, S., Friedlingstein, P., Grandpeix, J.-Y., Guez, L., Guilyardi, E., Hauglustaine, D., Hourdin,
754 F., Idelkadi, A., Ghattas, J., Joussaume, S., Kageyama, M., Krinner, G., Labetoulle, S., Lahellec, A.,
755 Lefebvre, M.-P., Lefevre, F., Levy, C., Li, Z.X., Lloyd, J., Lott, F., Madec, G., Mancip, M.,
756 Marchand, M., Masson, S., Meurdesoif, Y., Mignot, J., Musat, I., Parouty, S., Polcher, J., Rio, C.,

757 Schulz, M., Swingedouw, D., Szopa, S., Talandier, C., Terray, P., Viovy, N., Vuichard, N., 2013.
 758 Climate change projections using the IPSL-CM5 Earth System Model: from CMIP3 to CMIP5.
 759 Climate Dynamics 40, 2123–2165. <https://doi.org/10.1007/s00382-012-1636-1>
 760 Emanuel, K.A., David Neelin, J., Bretherton, C.S., 1994. On large-scale circulations in convecting
 761 atmospheres. Quarterly Journal of the Royal Meteorological Society 120, 1111–1143.
 762 <https://doi.org/10.1002/qj.49712051902>
 763 Evans, M.N., Tolwinski-Ward, S.E., Thompson, D.M., Anchukaitis, K.J., 2013. Applications of
 764 proxy system modeling in high resolution paleoclimatology. Quaternary Science Reviews 76, 16–28.
 765 <https://doi.org/10.1016/j.quascirev.2013.05.024>
 766 Farnsworth, A., Lunt, D.J., Robinson, S.A., Valdes, P.J., Roberts, W.H.G., Clift, P.D., Markwick, P.,
 767 Su, T., Wrobel, N., Bragg, F., Kelland, S.-J., Pancost, R.D., 2019. Past East Asian monsoon evolution
 768 controlled by paleogeography, not CO₂. Science Advances 5, eaax1697.
 769 <https://doi.org/10.1126/sciadv.aax1697>
 770 Feng, R., Poulsen, C.J., 2016. Refinement of Eocene lapse rates, fossil-leaf altimetry, and North
 771 American Cordilleran surface elevation estimates. Earth and Planetary Science Letters 436, 130–141.
 772 <https://doi.org/10.1016/j.epsl.2015.12.022>
 773 Fluteau, F., Ramstein, G., Besse, J., 1999. Simulating the evolution of the Asian and African
 774 monsoons during the past 30 Myr using an atmospheric general circulation model. Journal of
 775 Geophysical Research: Atmospheres 104, 11995–12018. <https://doi.org/10.1029/1999JD900048>
 776 Frauenfeld, O.W., 2005. Climate change and variability using European Centre for Medium-Range
 777 Weather Forecasts reanalysis (ERA-40) temperatures on the Tibetan Plateau. Journal of Geophysical
 778 Research 110. <https://doi.org/10.1029/2004JD005230>
 779 Gasson, E., Lunt, D.J., DeConto, R., Goldner, A., Heinemann, M., Huber, M., LeGrande, A.N.,
 780 Pollard, D., Sagoo, N., Siddall, M., Winguth, A., Valdes, P.J., 2014. Uncertainties in the modelled
 781 CO₂ threshold for Antarctic glaciation. Climate of the Past 10, 451–466. [https://doi.org/10.5194/cp-](https://doi.org/10.5194/cp-10-451-2014)
 782 10-451-2014
 783 Gough, D.O., 1981. Solar Interior Structure and Luminosity Variations, in: Domingo, V. (Ed.),
 784 Physics of Solar Variations. Springer Netherlands, Dordrecht, pp. 21–34.
 785 https://doi.org/10.1007/978-94-010-9633-1_4
 786 Grimm, G.W., Potts, A.J., 2016. Fallacies and fantasies: the theoretical underpinnings of the
 787 Coexistence Approach for palaeoclimate reconstruction. Climate of the Past 12, 611–622.
 788 <https://doi.org/10.5194/cp-12-611-2016>
 789 Guo, Z.T., Ruddiman, W.F., Hao, Q.Z., Wu, H.B., Qiao, Y.S., Zhu, R.X., Peng, S.Z., Wei, J.J., Yuan,

790 B.Y., Liu, T.S., 2002. Onset of Asian desertification by 22 Myr ago inferred from loess deposits in
791 China 416, 5.

792 Herman, A.B., Spicer, R.A., Aleksandrova, G.N., Yang, J., Kodrul, T.M., Maslova, N.P., Spicer,
793 T.E.V., Chen, G., Jin, J.-H., 2017. Eocene–early Oligocene climate and vegetation change in southern
794 China: Evidence from the Maoming Basin. *Palaeogeography, Palaeoclimatology, Palaeoecology* 479,
795 126–137. <https://doi.org/10.1016/j.palaeo.2017.04.023>

796 Herold, N., Buzan, J., Seton, M., Goldner, A., Green, J.A.M., Müller, R.D., Markwick, P., Huber, M.,
797 2014. A suite of early Eocene (~ 55 Ma) climate model boundary conditions. *Geoscientific Model*
798 *Development* 7, 2077–2090. <https://doi.org/10.5194/gmd-7-2077-2014>

799 Ho, S.L., Laepple, T., 2016. Flat meridional temperature gradient in the early Eocene in the
800 subsurface rather than surface ocean. *Nature Geoscience* 9, 606–610.
801 <https://doi.org/10.1038/ngeo2763>

802 Hourdin, F., Foujols, M.-A., Codron, F., Guemas, V., Dufresne, J.-L., Bony, S., Denvil, S., Guez, L.,
803 Lott, F., Ghattas, J., Braconnot, P., Marti, O., Meurdesoif, Y., Bopp, L., 2013. Impact of the LMDZ
804 atmospheric grid configuration on the climate and sensitivity of the IPSL-CM5A coupled model.
805 *Climate Dynamics* 40, 2167–2192. <https://doi.org/10.1007/s00382-012-1411-3>

806 Huber, M., Caballero, R., 2011. The early Eocene equable climate problem revisited. *Climate of the*
807 *Past* 7, 603–633. <https://doi.org/10.5194/cp-7-603-2011>

808 Huber, M., Goldner, A., 2012. Eocene monsoons. *Journal of Asian Earth Sciences* 44, 3–23.
809 <https://doi.org/10.1016/j.jseas.2011.09.014>

810 Hutchinson, D.K., de Boer, A.M., Coxall, H.K., Caballero, R., Nilsson, J., Baatsen, M., 2018. Climate
811 sensitivity and meridional overturning circulation in the late Eocene using GFDL CM2.1. *Climate of*
812 *the Past Discussions* 1–46. <https://doi.org/10.5194/cp-2017-161>

813 Inglis, G.N., Farnsworth, A., Lunt, D., Foster, G.L., Hollis, C.J., Pagani, M., Jardine, P.E., Pearson,
814 P.N., Markwick, P., Galsworthy, A.M.J., Raynham, L., Taylor, Kyle.W.R., Pancost, R.D., 2015.
815 Descent toward the Icehouse: Eocene sea surface cooling inferred from GDGT distributions:
816 DESCENT TOWARD THE ICEHOUSE. *Paleoceanography* 30, 1000–1020.
817 <https://doi.org/10.1002/2014PA002723>

818 Jagoutz, O., Royden, L., Holt, A.F., Becker, T.W., 2015. Anomalously fast convergence of India and
819 Eurasia caused by double subduction. *Nature Geoscience* 8, 475–478.
820 <https://doi.org/10.1038/ngeo2418>

821 Kageyama, M., Braconnot, P., Bopp, L., Caubel, A., Foujols, M.-A., Guilyardi, E., Khodri, M., Lloyd,
822 J., Lombard, F., Mariotti, V., Marti, O., Roy, T., Woillez, M.-N., 2013. Mid-Holocene and Last

823 Glacial Maximum climate simulations with the IPSL model—part I: comparing IPSL_CM5A to
824 IPSL_CM4. *Climate Dynamics* 40, 2447–2468. <https://doi.org/10.1007/s00382-012-1488-8>

825 Kapp, P., DeCelles, P.G., 2019. Mesozoic–Cenozoic geological evolution of the Himalayan-Tibetan
826 orogen and working tectonic hypotheses. *American Journal of Science* 319, 159–254.
827 <https://doi.org/10.2475/03.2019.01>

828 Kaya, M.Y., Dupont-Nivet, G., Proust, J., Roperch, P., Bougeois, L., Meijer, N., Frieling, J., Fioroni,
829 C., Özkan Altıner, S., Vardar, E., Barbolini, N., Stoica, M., Aminov, J., Mamtimin, M., Zhaojie, G.,
830 2019. Paleogene evolution and demise of the proto-Paratethys Sea in Central Asia (Tarim and Tajik
831 basins): Role of intensified tectonic activity at ca. 41 Ma. *Basin Research* 31, 461–486.
832 <https://doi.org/10.1111/bre.12330>

833 Krinner, G., Viovy, N., de Noblet-Ducoudré, N., Ogée, J., Polcher, J., Friedlingstein, P., Ciais, P.,
834 Sitch, S., Prentice, I.C., 2005. A dynamic global vegetation model for studies of the coupled
835 atmosphere-biosphere system: DVG M FOR COUPLED CLIMATE STUDIES. *Global*
836 *Biogeochemical Cycles* 19. <https://doi.org/10.1029/2003GB002199>

837 Lefebvre, V., Donnadieu, Y., Goddérès, Y., Fluteau, F., Hubert-Théou, L., 2013. Was the Antarctic
838 glaciation delayed by a high degassing rate during the early Cenozoic? *Earth and Planetary Science*
839 *Letters* 371–372, 203–211. <https://doi.org/10.1016/j.epsl.2013.03.049>

840 Levine, R.C., Turner, A.G., Marathayil, D., Martin, G.M., 2013. The role of northern Arabian Sea
841 surface temperature biases in CMIP5 model simulations and future projections of Indian summer
842 monsoon rainfall. *Climate Dynamics* 41, 155–172. <https://doi.org/10.1007/s00382-012-1656-x>

843 Li, X., Zhang, R., Zhang, Z., Yan, Q., 2018. Do climate simulations support the existence of East
844 Asian monsoon climate in the Late Eocene? *Palaeogeography, Palaeoclimatology, Palaeoecology*.
845 <https://doi.org/10.1016/j.palaeo.2017.12.037>

846 Licht, Alexis, Boura, A., De Franceschi, D., Ducrocq, S., Aung Naing Soe, Jaeger, J.-J., 2014. Fossil
847 woods from the late middle Eocene Pondaung Formation, Myanmar. *Review of Palaeobotany and*
848 *Palynology* 202, 29–46. <https://doi.org/10.1016/j.revpalbo.2013.12.002>

849 Licht, A., Boura, A., De Franceschi, D., Utescher, T., Sein, C., Jaeger, J.-J., 2015. Late middle Eocene
850 fossil wood of Myanmar: Implications for the landscape and the climate of the Eocene Bengal Bay.
851 *Review of Palaeobotany and Palynology* 216, 44–54. <https://doi.org/10.1016/j.revpalbo.2015.01.010>

852 Licht, A., van Cappelle, M., Abels, H.A., Ladant, J.-B., Trabucho-Alexandre, J., France-Lanord, C.,
853 Donnadieu, Y., Vandenberghe, J., Rigaudier, T., Lécuyer, C., Terry Jr, D., Adriaens, R., Boura, A.,
854 Guo, Z., Soe, A.N., Quade, J., Dupont-Nivet, G., Jaeger, J.-J., 2014. Asian monsoons in a late Eocene
855 greenhouse world. *Nature* 513, 501–506. <https://doi.org/10.1038/nature13704>

856 Lippert, P.C., Van Hinsbergen, D.J., Dupont-Nivet, G., 2014. Early Cretaceous to present latitude of
 857 the central proto-Tibetan Plateau: A paleomagnetic synthesis with implications for Cenozoic
 858 tectonics, paleogeography, and climate of Asia. *Geological Society of America Special Papers* 507,
 859 SPE507–01.
 860 Liu, Z., Pagani, M., Zinniker, D., DeConto, R., Huber, M., Brinkhuis, H., Shah, S.R., Leckie, R.M.,
 861 Pearson, A., 2009. Global Cooling During the Eocene-Oligocene Climate Transition. *Science* 323,
 862 1187–1190. <https://doi.org/10.1126/science.1166368>
 863 Lunt, D.J., Farnsworth, A., Loptson, C., Foster, G.L., Markwick, P., O'Brien, C.L.,
 864 Pancost, R.D., Robinson, S.A., Wrobel, N., 2016. Palaeogeographic controls on climate and proxy
 865 interpretation. *Climate of the Past* 12, 1181–1198. <https://doi.org/10.5194/cp-12-1181-2016>
 866 Lunt, D.J., Huber, M., Anagnostou, E., Baatsen, M.L.J., Caballero, R., DeConto, R., Dijkstra, H.A.,
 867 Donnadiou, Y., Evans, D., Feng, R., Foster, G.L., Gasson, E., von der Heydt, A.S., Hollis, C.J., Inglis,
 868 G.N., Jones, S.M., Kiehl, J., Kirtland Turner, S., Korty, R.L., Kozdon, R., Krishnan, S., Ladant, J.-
 869 B., Langebroek, P., Lear, C.H., LeGrande, A.N., Littler, K., Markwick, P., Otto-Bliesner, B., Pearson,
 870 P., Poulsen, C.J., Salzmann, U., Shields, C., Snell, K., St&aruml;z, M., Super, J., Tabor, C., Tierney, J.E.,
 871 Tourte, G.J.L., Tripathi, A., Upchurch, G.R., Wade, B.S., Wing, S.L., Winguth, A.M.E., Wright, N.M.,
 872 Zachos, J.C., Zeebe, R.E., 2017. The DeepMIP contribution to PMIP4: experimental design for model
 873 simulations of the EECO, PETM, and pre-PETM (version 1.0). *Geoscientific Model Development*
 874 10, 889–901. <https://doi.org/10.5194/gmd-10-889-2017>
 875 Ma, X., Jiang, H., Cheng, J., Xu, H., 2012. Spatiotemporal evolution of Paleogene palynoflora in
 876 China and its implication for development of the extensional basins in East China. *Review of*
 877 *Palaeobotany and Palynology* 184, 24–35. <https://doi.org/10.1016/j.revpalbo.2012.07.013>
 878 Ma, Y., Fan, M., Lu, Y., Liu, H., Zhang, S., Liu, X., 2019. Stable isotope record of middle Eocene
 879 summer monsoon and its instability in eastern China. *Global and Planetary Change* 175, 103–112.
 880 <https://doi.org/10.1016/j.gloplacha.2019.02.007>
 881 Madec, G., 2016. NEMO ocean engine 396.
 882 Meijer, N., Dupont-Nivet, G., Abels, H.A., Kaya, M.Y., Licht, A., Xiao, M., Zhang, Y., Roperch, P.,
 883 Poujol, M., Lai, Z., Guo, Z., 2019. Central Asian moisture modulated by proto-Paratethys Sea
 884 incursions since the early Eocene. *Earth and Planetary Science Letters* 510, 73–84.
 885 <https://doi.org/10.1016/j.epsl.2018.12.031>
 886 Molnar, P., Boos, W.R., Battisti, D.S., 2010. Orographic Controls on Climate and Paleoclimate of
 887 Asia: Thermal and Mechanical Roles for the Tibetan Plateau. *Annual Review of Earth and Planetary*
 888 *Sciences* 38, 77–102. <https://doi.org/10.1146/annurev-earth-040809-152456>

889 Najman, Y., Appel, E., Boudagher-Fadel, M., Bown, P., Carter, A., Garzanti, E., Godin, L., Han, J.,
 890 Liebke, U., Oliver, G., Parrish, R., Vezzoli, G., 2010. Timing of India-Asia collision: Geological,
 891 biostratigraphic, and palaeomagnetic constraints. *Journal of Geophysical Research* 115.
 892 <https://doi.org/10.1029/2010JB007673>
 893 Najman, Y., Bickle, M., BouDagher-Fadel, M., Carter, A., Garzanti, E., Paul, M., Wijbrans, J.,
 894 Willett, E., Oliver, G., Parrish, R., Akhter, S.H., Allen, R., Ando, S., Chisty, E., Reisberg, L., Vezzoli,
 895 G., 2008. The Paleogene record of Himalayan erosion: Bengal Basin, Bangladesh. *Earth and*
 896 *Planetary Science Letters* 273, 1–14. <https://doi.org/10.1016/j.epsl.2008.04.028>
 897 Peppe, D.J., Royer, D.L., Cariglino, B., Oliver, S.Y., Newman, S., Leight, E., Enikolopov, G.,
 898 Fernandez-Burgos, M., Herrera, F., Adams, J.M., Correa, E., Currano, E.D., Erickson, J.M., Hinojosa,
 899 L.F., Hoganson, J.W., Iglesias, A., Jaramillo, C.A., Johnson, K.R., Jordan, G.J., Kraft, N.J.B.,
 900 Lovelock, E.C., Lusk, C.H., Niinemets, Ü., Peñuelas, J., Rapson, G., Wing, S.L., Wright, I.J., 2011.
 901 Sensitivity of leaf size and shape to climate: global patterns and paleoclimatic applications. *New*
 902 *Phytologist* 190, 724–739. <https://doi.org/10.1111/j.1469-8137.2010.03615.x>
 903 Poulter, B., Ciais, P., Hodson, E., Lischke, H., Maignan, F., Plummer, S., Zimmermann, N.E., 2011.
 904 Plant functional type mapping for earth system models. *Geoscientific Model Development* 4, 993–
 905 1010. <https://doi.org/10.5194/gmd-4-993-2011>
 906 Privé, N.C., Plumb, R.A., 2007. Monsoon Dynamics with Interactive Forcing. Part I: Axisymmetric
 907 Studies. *Journal of the Atmospheric Sciences* 64, 1417–1430. <https://doi.org/10.1175/JAS3916.1>
 908 Quan, C., Liu, Y.-S. (Christopher), Utescher, T., 2012. Eocene monsoon prevalence over China: A
 909 paleobotanical perspective. *Palaeogeography, Palaeoclimatology, Palaeoecology* 365–366, 302–311.
 910 <https://doi.org/10.1016/j.palaeo.2012.09.035>
 911 Ramstein, G., Fluteau, F., Besse, J., Joussaume, S., 1997. Effect of orogeny, plate motion and land–
 912 sea distribution on Eurasian climate change over the past 30 million years. *Nature* 386, 788–795.
 913 <https://doi.org/10.1038/386788a0>
 914 Roe, G.H., Ding, Q., Battisti, D.S., Molnar, P., Clark, M.K., Garzione, C.N., 2016. A modeling study
 915 of the response of Asian summertime climate to the largest geologic forcings of the past 50 Ma:
 916 GEOLOGICAL CONTROLS ON ASIAN CLIMATE. *Journal of Geophysical Research:*
 917 *Atmospheres* 121, 5453–5470. <https://doi.org/10.1002/2015JD024370>
 918 Sarr, A., Sepulchre, P., Husson, L., 2019. Impact of the Sunda Shelf on the Climate of the Maritime
 919 Continent. *Journal of Geophysical Research: Atmospheres* 124, 2574–2588.
 920 <https://doi.org/10.1029/2018JD029971>
 921 Schmidt, G.A., 1999. Forward modeling of carbonate proxy data from planktonic foraminifera using

922 oxygen isotope tracers in a global ocean model. *Paleoceanography* 14, 482–497.
 923 <https://doi.org/10.1029/1999PA900025>
 924 Schouten, S., Hopmans, E.C., Sinninghe Damsté, J.S., 2013. The organic geochemistry of glycerol
 925 dialkyl glycerol tetraether lipids: A review. *Organic Geochemistry* 54, 19–61.
 926 <https://doi.org/10.1016/j.orggeochem.2012.09.006>
 927 Sepulchre, P., Caubel, A., Ladant, J.-B., Bopp, L., Boucher, O., Braconnot, P., Brockmann, P., Cozic,
 928 A., Donnadieu, Y., Estella-Perez, V., Ethé, C., Fluteau, F., Foujols, M.-A., Gastineau, G., Ghattas, J.,
 929 Hauglustaine, D., Hourdin, F., Kageyama, M., Khodri, M., Marti, O., Meurdesoif, Y., Mignot, J.,
 930 Sarr, A.-C., Servonnat, J., Swingedouw, D., Szopa, S., Tardif, D., 2019. IPSL-CM5A2. An Earth
 931 System Model designed for multi-millennial climate simulations. [https://doi.org/10.5194/gmd-2019-](https://doi.org/10.5194/gmd-2019-332)
 932 332
 933 Sewall, J.O., Sloan, L.C., 2006. Come a little bit closer: A high-resolution climate study of the early
 934 Paleogene Laramide foreland. *Geology* 34, 81. <https://doi.org/10.1130/G22177.1>
 935 Sewall, J.O., Sloan, L.C., Huber, M., Wing, S., 2000. Climate sensitivity to changes in land surface
 936 characteristics. *Global and Planetary Change* 26, 445–465. [https://doi.org/10.1016/S0921-](https://doi.org/10.1016/S0921-8181(00)00056-4)
 937 8181(00)00056-4
 938 Shukla, A., Mehrotra, R.C., Spicer, R.A., Spicer, T.E.V., Kumar, M., 2014. Cool equatorial terrestrial
 939 temperatures and the South Asian monsoon in the Early Eocene: Evidence from the Gurha Mine,
 940 Rajasthan, India. *Palaeogeography, Palaeoclimatology, Palaeoecology* 412, 187–198.
 941 <https://doi.org/10.1016/j.palaeo.2014.08.004>
 942 Sijp, W.P., von der Heydt, A.S., Dijkstra, H.A., Flögel, S., Douglas, P.M.J., Bijl, P.K., 2014. The role
 943 of ocean gateways on cooling climate on long time scales. *Global and Planetary Change* 119, 1–22.
 944 <https://doi.org/10.1016/j.gloplacha.2014.04.004>
 945 Sloan, L.C., Morrill, C., 1998. Orbital forcing and Eocene continental temperatures.
 946 *Palaeogeography, Palaeoclimatology, Palaeoecology* 144, 21–35. [https://doi.org/10.1016/S0031-](https://doi.org/10.1016/S0031-0182(98)00091-1)
 947 0182(98)00091-1
 948 Sorrel, P., Eymard, I., Leloup, P.-H., Maheo, G., Olivier, N., Sterb, M., Gournbet, L., Wang, G., Jing,
 949 W., Lu, H., Li, H., Yadong, X., Zhang, K., Cao, K., Chevalier, M.-L., Replumaz, A., 2017. Wet
 950 tropical climate in SE Tibet during the Late Eocene. *Scientific Reports* 7.
 951 <https://doi.org/10.1038/s41598-017-07766-9>
 952 Sperber, K.R., Annamalai, H., Kang, I.-S., Kitoh, A., Moise, A., Turner, A., Wang, B., Zhou, T.,
 953 2013. The Asian summer monsoon: an intercomparison of CMIP5 vs. CMIP3 simulations of the late
 954 20th century. *Climate Dynamics* 41, 2711–2744. <https://doi.org/10.1007/s00382-012-1607-6>

955 Spicer, R., Yang, J., Herman, A., Kodrul, T., Aleksandrova, G., Maslova, N., Spicer, T., Ding, L.,
 956 Xu, Q., Shukla, A., Srivastava, G., Mehrotra, R., Liu, X.-Y., Jin, J.-H., 2017. Paleogene monsoons
 957 across India and South China: Drivers of biotic change. *Gondwana Research* 49, 350–363.
 958 <https://doi.org/10.1016/j.gr.2017.06.006>
 959 Spicer, R.A., Yang, J., Herman, A.B., Kodrul, T., Maslova, N., Spicer, T.E.V., Aleksandrova, G., Jin,
 960 J., 2016. Asian Eocene monsoons as revealed by leaf architectural signatures. *Earth and Planetary*
 961 *Science Letters* 449, 61–68. <https://doi.org/10.1016/j.epsl.2016.05.036>
 962 Sun, X., Wang, P., 2005. How old is the Asian monsoon system?—Palaeobotanical records from
 963 China. *Palaeogeography, Palaeoclimatology, Palaeoecology* 222, 181–222.
 964 <https://doi.org/10.1016/j.palaeo.2005.03.005>
 965 Tada, R., Zheng, H., Clift, P.D., 2016. Evolution and variability of the Asian monsoon and its
 966 potential linkage with uplift of the Himalaya and Tibetan Plateau. *Progress in Earth and Planetary*
 967 *Science* 3. <https://doi.org/10.1186/s40645-016-0080-y>
 968 Tan, N., Ramstein, G., Dumas, C., Contoux, C., Ladant, J.-B., Sepulchre, P., Zhang, Z., De Schepper,
 969 S., 2017. Exploring the MIS M2 glaciation occurring during a warm and high atmospheric CO₂
 970 Pliocene background climate. *Earth and Planetary Science Letters* 472, 266–276.
 971 <https://doi.org/10.1016/j.epsl.2017.04.050>
 972 Tierney, J.E., Haywood, A.M., Feng, R., Bhattacharya, T., Otto-Bliesner, B.L., 2019. Pliocene
 973 Warmth Consistent With Greenhouse Gas Forcing. *Geophysical Research Letters* 46, 9136–9144.
 974 <https://doi.org/10.1029/2019GL083802>
 975 Tierney, J.E., Sinninghe Damsté, J.S., Pancost, R.D., Sluijs, A., Zachos, J.C., 2017. Eocene
 976 temperature gradients. *Nature Geoscience* 10, 538–539. <https://doi.org/10.1038/ngeo2997>
 977 Tierney, J.E., Tingley, M.P., 2018. BAYSPLINE: A New Calibration for the Alkenone
 978 Paleothermometer. *Paleoceanography and Paleoclimatology* 33, 281–301.
 979 <https://doi.org/10.1002/2017PA003201>
 980 Valcke, S., Budich, R., Carter, M., Guilyardi, E., Lautenschlager, M., Redler, R., Steenman-Clark,
 981 L., 2006. The PRISM software framework and the OASIS coupler 10.
 982 Valdes, P.J., Armstrong, E., Badger, M.P.S., Bradshaw, C.D., Bragg, F., Crucifix, M., Davies-
 983 Barnard, T., Day, J.J., Farnsworth, A., Gordon, C., Hopcroft, P.O., Kennedy, A.T., Lord, N.S., Lunt,
 984 D.J., Marzocchi, A., Parry, L.M., Pope, V., Roberts, W.H.G., Stone, E.J., Tourte, G.J.L., Williams,
 985 J.H.T., 2017. The BRIDGE HadCM3 family of climate models: HadCM3@Bristol v1.0.
 986 *Geoscientific Model Development* 10, 3715–3743. <https://doi.org/10.5194/gmd-10-3715-2017>
 987 van Hinsbergen, D.J.J., Lippert, P.C., Dupont-Nivet, G., McQuarrie, N., Doubrovine, P.V., Spakman,

988 W., Torsvik, T.H., 2012. Greater India Basin hypothesis and a two-stage Cenozoic collision between
989 India and Asia. *Proceedings of the National Academy of Sciences* 109, 7659–7664.
990 <https://doi.org/10.1073/pnas.1117262109>

991 Wang, B., Ding, Q., 2008. Global monsoon: Dominant mode of annual variation in the tropics.
992 *Dynamics of Atmospheres and Oceans* 44, 165–183.
993 <https://doi.org/10.1016/j.dynatmoce.2007.05.002>

994 Wang, B., LinHo, 2002. Rainy Season of the Asian–Pacific Summer Monsoon*. *Journal of Climate*
995 15, 386–398. [https://doi.org/10.1175/1520-0442\(2002\)015<0386:RSOTAP>2.0.CO;2](https://doi.org/10.1175/1520-0442(2002)015<0386:RSOTAP>2.0.CO;2)

996 Wang, C., Dai, J., Zhao, X., Li, Y., Graham, S.A., He, D., Ran, B., Meng, J., 2014. Outward-growth
997 of the Tibetan Plateau during the Cenozoic: A review. *Tectonophysics* 621, 1–43.
998 <https://doi.org/10.1016/j.tecto.2014.01.036>

999 Wang, D., Lu, S., Han, S., Sun, X., Quan, C., 2013. Eocene prevalence of monsoon-like climate over
1000 eastern China reflected by hydrological dynamics. *Journal of Asian Earth Sciences* 62, 776–787.
1001 <https://doi.org/10.1016/j.jseas.2012.11.032>

1002 Wang, Q., Spicer, R.A., Yang, J., Wang, Y.-F., Li, C.-S., 2013. The Eocene climate of China, the
1003 early elevation of the Tibetan Plateau and the onset of the Asian Monsoon. *Global Change Biology*
1004 19, 3709–3728. <https://doi.org/10.1111/gcb.12336>

1005 Webster, P.J., Yang, S., 1992. Monsoon and Enso: Selectively Interactive Systems. *Quarterly Journal*
1006 *of the Royal Meteorological Society* 118, 877–926. <https://doi.org/10.1002/qj.49711850705>

1007 Wei, H.-H., Bordoni, S., 2016. On the Role of the African Topography in the South Asian Monsoon.
1008 *Journal of the Atmospheric Sciences* 73, 3197–3212. <https://doi.org/10.1175/JAS-D-15-0182.1>

1009 Westerweel, J., Roperch, P., Licht, A., Dupont-Nivet, G., Win, Z., Poblete, F., Ruffet, G., Swe, H.H.,
1010 Thi, M.K., Aung, D.W., 2019. Burma Terrane part of the Trans-Tethyan arc during collision with
1011 India according to palaeomagnetic data. *Nature Geoscience* 12, 863–868.
1012 <https://doi.org/10.1038/s41561-019-0443-2>

1013 Williams, M., 2007. Deep-time perspectives on climate change: marrying the signal from computer
1014 models and biological proxies., Geological Society of London. ed.

1015 Zhang, R., Jiang, D., Ramstein, G., Zhang, Z., Lippert, P.C., Yu, E., 2018. Changes in Tibetan Plateau
1016 latitude as an important factor for understanding East Asian climate since the Eocene: A modeling
1017 study. *Earth and Planetary Science Letters* 484, 295–308. <https://doi.org/10.1016/j.epsl.2017.12.034>

1018 Zhang, S., Wang, B., 2008. Global summer monsoon rainy seasons. *International Journal of*
1019 *Climatology* 28, 1563–1578. <https://doi.org/10.1002/joc.1659>

1020 Zhang, Z., Flatøy, F., Wang, H., Bethke, I., Bentsen, M., Guo, Z., 2012. Early Eocene Asian climate

1021 dominated by desert and steppe with limited monsoons. *Journal of Asian Earth Sciences* 44, 24–35.
 1022 <https://doi.org/10.1016/j.jseas.2011.05.013>
 1023 Zhang, Z., Wang, H., Guo, Z., Jiang, D., 2007. What triggers the transition of palaeoenvironmental
 1024 patterns in China, the Tibetan Plateau uplift or the Paratethys Sea retreat? *Palaeogeography,*
 1025 *Palaeoclimatology, Palaeoecology* 245, 317–331. <https://doi.org/10.1016/j.palaeo.2006.08.003>
 1026 Zhisheng, A., Guoxiong, W., Jianping, L., Youbin, S., Yimin, L., Weijian, Z., Yanjun, C., Anmin,
 1027 D., Li, L., Jiangyu, M., Hai, C., Zhengguo, S., Liangcheng, T., Hong, Y., Hong, A., Hong, C., Juan,
 1028 F., 2015. Global Monsoon Dynamics and Climate Change. *Annual Review of Earth and Planetary*
 1029 *Sciences* 43, 29–77. <https://doi.org/10.1146/annurev-earth-060313-054623>
 1030 Zhu, J., Poulsen, C.J., Tierney, J.E., 2019. Simulation of Eocene extreme warmth and high climate
 1031 sensitivity through cloud feedbacks. *Science Advances* 5, eaax1874.
 1032 <https://doi.org/10.1126/sciadv.aax1874>
 1033 Ziegler, A., Eshel, G., Rees, P.M., Rothfus, T., Rowley, D., Sunderlin, D., 2003. Tracing the tropics
 1034 across land and sea: Permian to present. *Lethaia* 36, 227–254.
 1035 <https://doi.org/10.1080/00241160310004657>
 1036 Zoura, D., Hill, D.J., Dolan, A.M., Hunter, S.J., Tang, Z., Haywood, A.M., 2019. Atmospheric carbon
 1037 dioxide, ice sheet and topographic constraints on palaeo moisture availability in Asia. *Earth and*
 1038 *Planetary Science Letters* 519, 12–27. <https://doi.org/10.1016/j.epsl.2019.04.035>
 1039
 1040

Mis en forme : Interligne : Multiple 1,15 li

Supprimé: Abels, H.A., Dupont-Nivet, G., Xiao, G., Bosboom, R., Krijgsman, W., 2011. Step-wise change of Asian interior climate preceding the Eocene–Oligocene Transition (EOT). *Palaeogeography, Palaeoclimatology, Palaeoecology* 299, 399–412. <https://doi.org/10.1016/j.palaeo.2010.11.028>
 Akhmetiev, M.A., Zaporozhets, N.I., 2014. Paleogene events in Central Eurasia: their role in the flora and vegetation cover evolution, migration of phytochore boundaries, and climate changes. *Stratigraphy and Geological Correlation* 22, 312–335. <https://doi.org/10.1134/S0869593814030022>
 Akhmetiev, M.A., Beniamovski, V.N., 2006. The Paleocene and Eocene in the Russian part of West Eurasia. *Stratigraphy and Geological Correlation* 14, 49–72. <https://doi.org/10.1134/S0869593806010047>
 Anagnostou, E., John, E.H., Edgar, K.M., Foster, G.L., Ridgwell, A., Inglis, G.N., Pancost, R.D., Lunt, D.J., Pearson, P.N., 2016. Changing atmospheric CO₂ concentration was the primary driver of early Cenozoic climate. *Nature* 533, 380–384. <https://doi.org/10.1038/nature17423>
 Baatsen, M., van Hinsbergen, D.J.J., von der Heydt, A.S., Dijkstra, H.A., Sluijs, A., Abels, H.A., Bijl, P.K., 2016. Reconstructing geographical boundary conditions for palaeoclimate modelling during the Cenozoic. *Climate of the Past* 12, 1635–1644. <https://doi.org/10.5194/cp-12-1635-2016>
 Baatsen, M., von der Heydt, A.S., Huber, M., Kliphuis, M.A., Bijl, P.K., Sluijs, A., Dijkstra, H.A., 2018. Equilibrium state and sensitivity of the simulated middle-to-late Eocene climate. *Climate of the Past Discussions* 1–49. <https://doi.org/10.5194/cp-2018-43>
 Bannon, P.R., 1979. On the Dynamics of the East African Jet. I: Simulation of Mean Conditions for July. *Journal of the Atmospheric Sciences* 36, 2139–2152. [https://doi.org/10.1175/1520-0469\(1979\)036<2139:OTDOTE>2.0.CO;2](https://doi.org/10.1175/1520-0469(1979)036<2139:OTDOTE>2.0.CO;2)
 Beerling, D.J., Royer, D.L., 2011. Convergent cenozoic CO₂ history. *Nature Geoscience* 4, 418–420. <https://doi.org/10.1038/nature08707>
 Boos, W.R., Kuang, Z., 2010. Dominant control of the South Asian monsoon by orographic insulation versus plateau heating. *Nature* 463, 218–222. <https://doi.org/10.1038/nature08707>
 Bosboom, R., Mandic, O., Dupont-Nivet, G., Proust, J.-N., Ormukov, C., Aminov, J., 2017. Late Eocene palaeogeography of the proto-Paratethys Sea in Central Asia (NW China, southern Kyrgyzstan and SW Tajikistan). *Geological Society, London, Special Publications* 427, 565–588. <https://doi.org/10.1144/SP427.11>
 Botsyun, S., Sepulchre, P., Donnadiou, Y., Risi, C., Licht, A., Caves Rugenstein, J.K., 2019. Revised paleoaltimetry data show low Tibetan Plateau elevation during the Eocene. *Science* 363, eaq1436. <https://doi.org/10.1126/science.aq1436>
 Boucot, A.J., Xu, C., Scotese, C.R., Morley, R.J., 2013. Phanerozoic Paleoclimate: An Atlas of Lithologic Indicators of Climate. SEPM (Society for Sedimentary Geology), Tulsa, Oklahoma, U.S.A. <https://doi.org/10.2110/sepmcsp.11>
 Bougeois, L., Dupont-Nivet, G., de Rafélis, M., Tindall, J.C., Proust, J.-N., Reichart, G.-J., de Nooijer, L.J., Guo, Z., Ormukov, C., 2018. Asian monsoons and aridification response to Paleogene sea retreat and Neogene westerly shielding indicated by seasonality in Paratethys oysters. *Earth and Planetary Science Letters* 485, 99–110. <https://doi.org/10.1016/j.epsl.2017.12.036>

... [1]

Mis en forme : Police : 10 pt

